ESC Cardiovascular Research (2026) **00**, 1–17
https://doi.org/10.1093/cvr/cvag152

CKD disrupts cardiac energy metabolism and aggravates cardiac inflammation, oxidative stress, and dysfunction post-infarction

Corinna Schulte[1†], Julia Wollenhaupt[1†], Sina Hourtz [1†], Eva Harlacher[1†], Julia Moellmann[2], Carolina Victoria Cruz Junho[1], Michael Kohlhaas [3], Vera Jankowski[1], Han Jin[4,5], Martin Reugels [2], Sidrah Maryam[6], Franca Hausmann[3], Dickson W.L. Wong [7], Emiel P.C. van der Vorst[1,8,9,10], Martin Berger [2], Sonja Vondenhoff[1], Berkan Kurt [2], Bart Ghesquière[11], Constanze Mueller[12], Ulrike Schulze-Späte[13], Philippe Schmitt-Kopplin[12,14], Erik A.L. Biessen[4,8], Leticia Prates-Roma[15], Moritz Biener[16], Evangelos Giannitsis [16], Hugo A. Katus [16], Stefan Schunk[17], Danilo Fliser[17], Katharina Marx-Schütt [2], Michael Lehrke[2], Rafael Kramann [6], Florian Kahles [2], Peter Boor [7], Claudia Goettsch [2,18], Sikander Hayat [6], Joachim Jankowski [1,4,8], Christoph Maack [3], Yvonne Döring [10,19,20,21], Nikolaus Marx [2,8], and Heidi Noels [1,8,22*]

[1]Institute for Molecular Cardiovascular Research (IMCAR), Uniklinik RWTH Aachen, Pauwelsstraße 30, Aachen 52074, Germany; [2]Department of Internal Medicine I, Cardiology, Uniklinik RWTH Aachen, Aachen, Germany; [3]Department of Translational Research, Comprehensive Heart Failure Center (CHFC), University Hospital Würzburg, Würzburg, Germany; [4]Department of Pathology, Cardiovascular Research Institute Maastricht (CARIM), Maastricht University, Maastricht, the Netherlands; [5]Central Laboratory, Tianjin Medical University General Hospital, Tianjin, China; [6]Department of Medicine II, Uniklinik RWTH Aachen, Aachen, Germany; [7]Institute of Pathology, Uniklinik RWTH Aachen, Aachen, Germany; [8]Aachen-Maastricht Institute for Cardiorenal Research (AMICARE), Uniklinik RWTH Aachen, Aachen, Germany; [9]Interdisciplinary Center for Clinical Research (IZKF), RWTH Aachen University, Aachen, Germany; [10]Institute for Cardiovascular Prevention (IPEK), Ludwig-Maximilians-University Munich, Munich, Germany; [11]Metabolomics Core Facility Leuven, VIB VIB Technologies, Leuven, Belgium; [12]Research Unit Analytical BioGeoChemistry, Helmholtz Zentrum München, Neuherberg, Germany; [13]Section of Geriodontics, Department of Conservative Dentistry and Periodontics, University Hospital Jena, Jena, Germany; [14]Analytical Food Chemistry, Technical University of Munich, Freising, Germany; [15]Biophysics Department, Zentrum für Human- und Molekularbiologie—Universität des Saarlandes, Saarbrücken, Germany; [16]Department of Internal Medicine III, Cardiology, Angiology and Pulmonology, Heidelberg University Hospital, Heidelberg, Germany; [17]Department of Internal Medicine IV, Renal and Hypertensive Disease & Transplant Centre, Saarland University Medical Centre, Homburg, Germany; [18]Institute of Physiology, Faculty of Medicine Carl Gustav Carus, Technical University Dresden, Dresden, Germany; [19]Department of Angiology, Swiss Cardiovascular Center, Inselspital, Bern University Hospital, University of Bern, Bern, Switzerland; [20]Department for BioMedical Research (DBMR), University of Bern, Bern, Switzerland; [21]DZHK (German Centre for Cardiovascular Research), Partner Site Munich Heart Alliance, Munich, Germany; and [22]Department of Biochemistry, Cardiovascular Research Institute Maastricht (CARIM), Maastricht University, PO Box 616, 6200 MD Maastricht, the Netherlands

Received 12 March 2026; accepted 5 April 2026; online publish-ahead-of-print 24 July 2026

Time of primary review: 20 days

Aims Patients with chronic kidney disease (CKD) display a reduced survival following myocardial infarction (MI). As the underlying mechanisms remain unclear, we examined the impact of CKD on cardiac remodeling and function post-MI using a mouse model of adenine-induced CKD.

Methods and results After MI, CKD mice showed a stronger cardiac dysfunction compared to non-CKD controls. While immunohistochemical and immunofluorescence analyses did not reveal changes in cardiomyocyte apoptosis, infarction size, or myofibroblast content, CKD mice exhibited an increased number of circulating myeloid cells post-infarction and more

* Corresponding author. Tel: +49 241 8037147, Fax: +49 241 803380580, E-mail: hnoels@ukaachen.de
† Shared first authorship.

neutrophil infiltration in the heart. Combining RNAseq, untargeted kinome profiling, western blotting, and mass spectrometry revealed that post-MI, CKD enhanced cardiac oxidative stress and the acute stress complex S100A8/A9 in circulation and the heart, and enforced cardiac MAP-kinase p38 activation and NR4A1 phosphorylation as pathways underlying cardiomyocyte dysfunction. S100A8/A9 also exerted an acute detrimental impact on calcium flux and sarcomere shortening in cardiomyocytes *ex vivo*. Increased myeloid cell-derived S100A8/A9 expression was confirmed in the infarcted human heart by single-nucleus RNAseq, and CKD patients had higher post-infarction S100A8/A9 levels compared to patients without kidney dysfunction. Furthermore, integrating metabolomics, RNAseq, and mitochondrial analysis uncovered a disturbed cardiac metabolism with impaired glycolysis, a reduced glycerol-3-phosphate-shuttle, and a reduced Coenzyme A-bioavailability in CKD vs. non-CKD mice post-MI. These alterations were associated with poorer cardiac performance post-MI, without intrinsic defects in mitochondrial function observed.

Conclusion Our study reveals innate immune activation, inflammation, oxidative stress, and metabolic alterations indicative of reduced glycolytic entry and CoA bioavailability along with aggravated cardiac dysfunction post-MI in CKD compared to non-CKD conditions, independent of infarct size, and with poorer cardiac performance in CKD associated with the cardiac metabolic alterations. Combined, this could contribute to the worsened outcome of CKD patients post-MI and reveals cardiac metabolism in CKD as an interesting translational research target.

Graphical Abstract

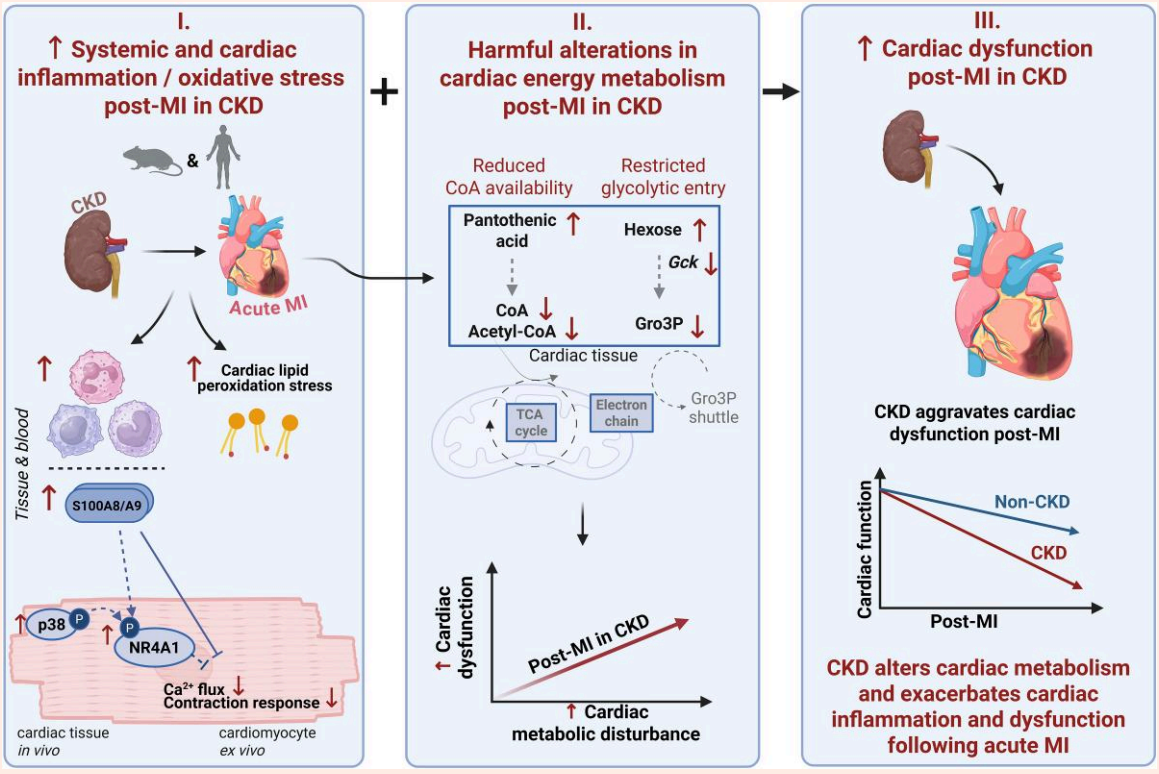

Keywords Chronic kidney disease • Cardiovascular disease • Myocardial infarction • Cardiomyocytes • Metabolism • Glycolysis • Inflammation • Innate immunity

1. Introduction

With a global prevalence of ~13.4%,[1] chronic kidney disease (CKD) imposes a high socio-economic burden.[2] Beyond kidney damage and a reduced kidney filtration function, CKD patients suffer from a highly increased cardiovascular risk. Cardiovascular disease (CVD) accounts for ~40% of all deaths in patients with advanced CKD,[3–5] with ischemic heart disease the most common cause of cardiovascular death in CKD.[3] CKD patients show more progressed atherosclerosis as the main underlying cause of myocardial infarction (MI),[6] but also a reduced survival post-MI with a higher risk of mortality and non-fatal cardiac events with declining kidney function.[7,8] Yet, the underlying mechanisms remain largely unclear.

MI triggers an inflammatory response in the heart with recruitment of myeloid cells including neutrophils and monocytes and the production of pro-inflammatory mediators, ultimately contributing to a detrimental remodeling of the heart post-MI.[9] Also, the heart undergoes metabolic alterations post-MI, which contribute to the development of heart failure.[10] The healthy heart mainly depends on fatty acid metabolism for cardiac energy requirements, but ischemic conditions reduce the heart's ability to oxidize fatty acids via the citric acid cycle and oxidative phosphorylation, and instead shift its dependence to glycolysis.[10,11]

Mouse models of CKD have intensively been used to analyze the impact of CKD on the heart, as summarized in detail in our systematic review and meta-analysis.[12,13] Most of these studies focused on uremic cardiomyopathy, i.e. cardiac remodeling in advanced CKD in the absence of infarction. This revealed CKD to trigger cardiac inflammation and oxidative stress, fibrosis, and cardiac functional alterations,[12–18] however, with high variability in observed changes between studies due to a combination of differences in the CKD model, mouse strain dependency, CKD duration as well as the presence of additional cardiovascular risk factors.[12,13] Our own comparison of cardiac remodeling of the non-infarcted heart in eight different CKD mouse models revealed pro-oxidative priming in the myocardium in CKD, however, without other signs of cardiac remodeling or cardiac functional changes in these CKD mouse models.[19,20]

Therefore, we next investigated in this study the effects of CKD on cardiac remodeling and function post-MI and provide insights into the underlying pathophysiological mechanisms using a combination of RNAseq, kinome activity profiling, mass spectrometry, and metabolomics.

2. Methods

A detailed description is available in Supplementary material online, *Supplemental Methods*.

2.1 Animals and organ isolation

Studies were performed with 8–10-week-old male C57BL/6J Apolipoprotein E-deficient (*ApoE*$^{-/-}$) mice. All procedures were approved by LAVE Nordrhein Westfalen (81-02.04.2017.A504; 81-02.04.2023.A163) and comply with local and national guidelines and those from Directive 2010/63/EU of the European Parliament on the protection of animals used for scientific purposes. To investigate the impact of CKD on the heart after myocardial infarction (MI) in a context of high cardiometabolic risk, CKD was induced in hyperlipidemic *ApoE*$^{-/-}$ mice after an initial 4 weeks of western-type diet (WD) by feeding an adenine-rich western-type diet (WD) supplemented with 0.3% adenine for 10 days (CKD induction phase), followed by a WD supplemented with 0.15% adenine (CKD maintenance phase) thereafter, as we previously characterized in detail.[19] Non-CKD controls received the same diet without adenine. Myocardial infarction was induced by permanent ligation of the proximal left anterior descending artery, 4 or 7 days after start of the CKD maintenance phase (or at the corresponding time point for the non-CKD control group). Thirty minutes before surgery, the mice received analgesia with buprenorphine (0.1 mg/kg, subcutaneous injection). The mice were anesthetized by intraperitoneal injection of ketamine (100 mg/kg) and xylazine (10 mg/kg). During surgical procedures, anesthesia was maintained with 0.5 vol% isoflurane using a rodent respirator. The thorax was opened under additional local analgesia with 0.2% lidocaine. Analgesia was continued using buprenorphine daily until five days after surgery (0.1 mg/kg every 8 h; subcutaneous injection) or the mice received the injections only in the first 12 h after surgery every 4 h and then analgesia was continued for three days via buprenorphine-supplemented drinking water (0.009 mg/mL). Where indicated, an additional blockade of CCL6 or CCL9 was performed by intraperitoneal injection of a blocking antibody. In three dose-finding experiments, the S100A8/A9 complex was pharmacologically targeted *in vivo* by treating mice with Paquinimod (ABR-215757) or ABR-238901. Kidney function was analyzed by quantification of creatinine and urea in serum. Non-invasive blood pressure measurements were performed using the tail-cuff method. Blood sampling was performed through retro-orbital bleeding under isoflurane (2–3 vol%) anesthesia. Cardiac function was quantified by invasive Millar catheter analysis in baseline and stressed condition (5 µg/g body weight via intraperitoneal injection). The procedure was performed under anesthesia via an intraperitoneal injection of ketamine (100 mg/kg body weight) and xylazine (10 mg/kg) and analgesia with buprenorphine (0.1 mg/kg, subcutaneous injection). At sacrifice, still under anesthesia, death was confirmed by exsanguination. Alternatively, mice were sacrificed for blood and organ isolation by exsanguination by cardiac puncture under anesthesia via an intraperitoneal injection of ketamine (100 mg/kg body weight) and xylazine (10 mg/kg). Organs were isolated and processed for histological analysis or—after separating infarct area and left ventricular (LV) remote area—for RNA sequencing, protein analysis, or metabolomics to study potential pathophysiological processes.

2.2 Tissue, cell, and protein analysis

Cardiac transversal and kidney longitudinal tissue sections were prepared from fixed, paraffin-embedded tissue for histological analyses, including Acid Fuchsin Orange G (renal fibrosis), periodic acid-Schiff (renal tubular injury), and Gomori's 1-step trichrome (cardiac infarction size), as well as immunofluorescence analyses quantifying tissue content of cells positive for MAC3, myeloperoxidase, CD31, smooth muscle actin (SMA), or Ki67. Apoptotic cells were detected by terminal deoxynucleotidyl nick-end labeling (TUNEL).

Monocyte and neutrophil counts in blood were determined using a Hematology Analyzer with additional differential blood analysis to distinguish leucocyte subsets through Wright's stain. Flow cytometry was used to quantify surface marker expression on blood neutrophils as well as profiling of hematopoietic cells in heart tissue, the latter with gating for leucocytes (CD45+), neutrophils (CD45+ CD11b + CD115− Gr1+), monocytes (CD45+ CD11b + CD115+), and tissue macrophages (CD45+ CD11b + F4/80+) with subsets M1 (CD206−) or M2 (CD206+).

Proteins were isolated from tissue using a non-denaturing cell lysis buffer supplemented with a protease and phosphatase inhibitor cocktail. Protein content was quantified by ELISA (CCL6, CCL9, and S100A8/A9 heterodimer) or by western blot analysis (P-p38). Lipid peroxidation status (as combined levels of malondialdehyde and 4-hydroxyalkenals) was quantified using the Lipid Peroxidation Assay (G-Biosciences) and normalized to the protein content in the analyzed tissue.

A multiplex kinome activity profiling of serine-threonine kinases (STK) in cardiac LV tissue extracts was performed using the PamChip® microarray platform and BioNavigator software to identify phosphorylated substrates and upstream kinases. Phosphorylation of NR4A1 was validated in cardiac LV tissue extracts using matrix-assisted-laser-desorption/ionization-time-of-flight-mass spectrometry (MALDI-TOF/TOF) by quantifying the phosphorylated 'LPSKPK' peptide of NR4A1 (at Serine 354) relative to internal standard.

2.3 RNA sequencing and metabolomics analysis of mouse tissue

For bulk RNA sequencing, RNA was isolated from cardiac LV tissue using a tissue lyzer and a combination of Trizol and an RNeasy

Micro Kit (Qiagen) with on column-DNase treatment. Paired-end RNA sequencing was performed at Genewiz (GENEWIZ GmbH, Germany) using Illumina NovaSeq 6000 with included quality controls and adapter trimming. Gene level read counts were quantified and assembled using the R package Rsubread, and differential expression analysis was performed using the R package DESeq2 to reveal differentially expressed genes (DEGs) in 'CKD + MI' mice compared to the 'Control + MI' group. *P*-values were adjusted by the Benjamini–Hochberg procedure ($P_{adjusted}$). Data were visualized in a volcano plot. Pathway analysis was performed using the gene ontology (GO) database and the R package clusterProfiler, and DEGs of interest were selected based on criteria of the expression level, adjusted *P*-value, and biological function. The RNAseq data have been deposited in the Gene Expression Omnibus (GEO) database (GSE283464).

Untargeted metabolomics on cardiac LV tissue was performed with direct-injection electrospray ionization Fourier transform ion cyclotron resonance mass spectrometry (ESI FT-ICR-MS). Mass spectra were internally calibrated against a set of endogenous metabolites using Data Analysis software (Bruker Daltonics). The data were normalized against the total ion count, and zero imputation by randomly chosen minimums was applied. The software Metaboanalyst (https://www.metaboanalyst.ca) was used for calculation of fold change and statistical analysis, pathway analysis, and data visualization, including heat map generation.

Targeted metabolomics was performed with a Dionex UltiMate 3000 LC System coupled to a Q Exactive Orbitrap mass spectrometer. Data collection was performed using the Xcalibur software (Thermo Scientific), and data analyses were performed by integrating the peak areas (El-Maven). After subtraction of intensity of the blanks, data were normalized to tissue weight before statistical analysis.

2.4 *Ex vivo* cardiomyocyte function analysis

Studies were performed with 14-week-old male C57BL/6J mice. All procedures were approved by RUF Würzburg (RUF 55.2.2-2532-2-1755) and comply with local and national guidelines and those from Directive 2010/63/EU of the European Parliament on the protection of animals used for scientific purposes. For isolation of cardiomyocytes, the mice were put under analgesia by buprenorphine (0.1 mg/kg, subcutaneous injection) and anesthesia with isoflurane (3–5 vol%). Mice were heparinized (500 IU/kg heparin, s.c.) before organ harvesting. Cardiomyocytes were then isolated from the hearts in a Langendorff perfusion system, and Ca^{2+}-flux and sarcomere shortening were analyzed using a customized automated IonOptix setup (DZHI, Würzburg) and evaluated using IonWizard Software (IonOptix) as described previously.[21–23] Before cardiomyocyte analysis, cells were stimulated at 37°C with 1 µg/mL of the S100A8/A9 heterodimer (in PBS) in Normal Tyrode's solution for 15 and 30 min, or with PBS as unstimulated controls.

2.5 Patient cohorts and human single-nucleus (sn)-RNAseq

Levels of the S100A8/A9 protein complex were analyzed by ELISA in patient cohorts. A first cohort included 103 patients with stable coronary artery disease and estimated glomerular filtration rate (eGFR) ≥ 30 [thus excluding patients with severe loss of kidney function (CKD stage 4) or end-stage renal dysfunction (CKD stage 5)]. Patients were recruited while admitted to the Department of Internal Medicine 1 at the University Hospital Aachen, with comparison of patients with kidney dysfunction (CKD3, 30 ≤ eGFR<60) vs. those without (eGFR≥60). Also, we analyzed S100A8/A9 serum levels in a cohort of CKD patients in stage 4–5 (eGFR<30, recruited at the Saarland University Hospital) compared to healthy controls as well as in 1390 patients with acute myocardial infarction (recruited at the University Hospital Heidelberg) comparing patients with kidney dysfunction (eGFR<60) vs. those without (eGFR≥60). All studies comply with the Declaration of Helsinki, and the local ethics committee approved the research protocol. All patients provided written informed consent.

Expression of selected genes was also analyzed in human infarcted hearts using snRNA-seq data of in total 31 samples from 23 individuals, including four non-transplanted donor hearts as controls, as previously described.[24] Raw counts were log-normalized using *normalize_total* and *log1p* functions in Scanpy (version = 1.10.3). The cell scores for the individual genes were calculated by using *score_genes* in Scanpy. The expression values visualized in UMAPs are cell_scores, scaled to be between the minimum and maximum expression value of that gene for visualization. Dot plots were generated using dot plot function in Scanpy.

2.6 Statistics

Data are presented as means ± standard deviation (SD). All statistical data analyses and graph preparation were performed using GraphPad Prism (Version 10.4.-10.6). Statistics included one-way ANOVA with Dunnett's multiple comparisons test; the non-parametric Kruskal–Wallis test with Dunn's multiple comparisons test; two-way ANOVA with Sidak's post-test for multiple comparison without or with matching values; Student's *t*-test (unpaired, one- or two-tailed, without or with Welch correction) for two-group comparisons with normal distribution and without timing variables; and Mann–Whitney test for two-group comparisons without normal distribution, as appropriate. Outlier exclusion was performed based on the Grubbs test in GraphPad, as indicated in the figure legends. Correlation analysis was performed by determining the Pearson correlation coefficients for normally divided datasets. *P*-values are added in the figures. Detailed information on statistical analysis is provided in the figure legends.

3. Results

3.1 CKD aggravates cardiac dysfunction after myocardial infarction

To investigate the impact of CKD on the heart after myocardial infarction (MI) in the context of high cardiometabolic risk, CKD was induced in hyperlipidemic *ApoE*$^{-/-}$ mice by feeding an adenine-rich western-type diet (WD), after which MI was induced by ligation of the left anterior descending artery. Non-CKD controls received the same WD without adenine and were also subjected to MI (*Figure 1A*). Whereas the CKD induction protocol did not induce mortality, mortality after MI-induction was on average 5% for non-CKD and 20% for CKD mice.

Induction of CKD in the adenine-fed mice was confirmed by significantly increased levels of creatinine and urea in blood (see Supplementary material online, *Table S1*). Additionally, kidneys of adenine-fed mice showed strong fibrosis as well as severe tubular injury and infiltration of immune cells (see Supplementary material online, *Figure S1A–C*).

When analyzing cardiac function with Millar catheter analysis, no differences were observed between CKD and non-CKD conditions in the absence of MI induction (see Supplementary material online, *Figure S2A*), as previously reported by us.[19] Instead, LV contractility—indicated by maximal dP/dT—was significantly reduced in CKD compared to non-CKD mice from one-week post-MI onward in resting conditions and from one day post-MI onward under dobutamine stress (*Figure 1B*). Also, the systolic contractile reserve showed a minor but significant reduction in CKD

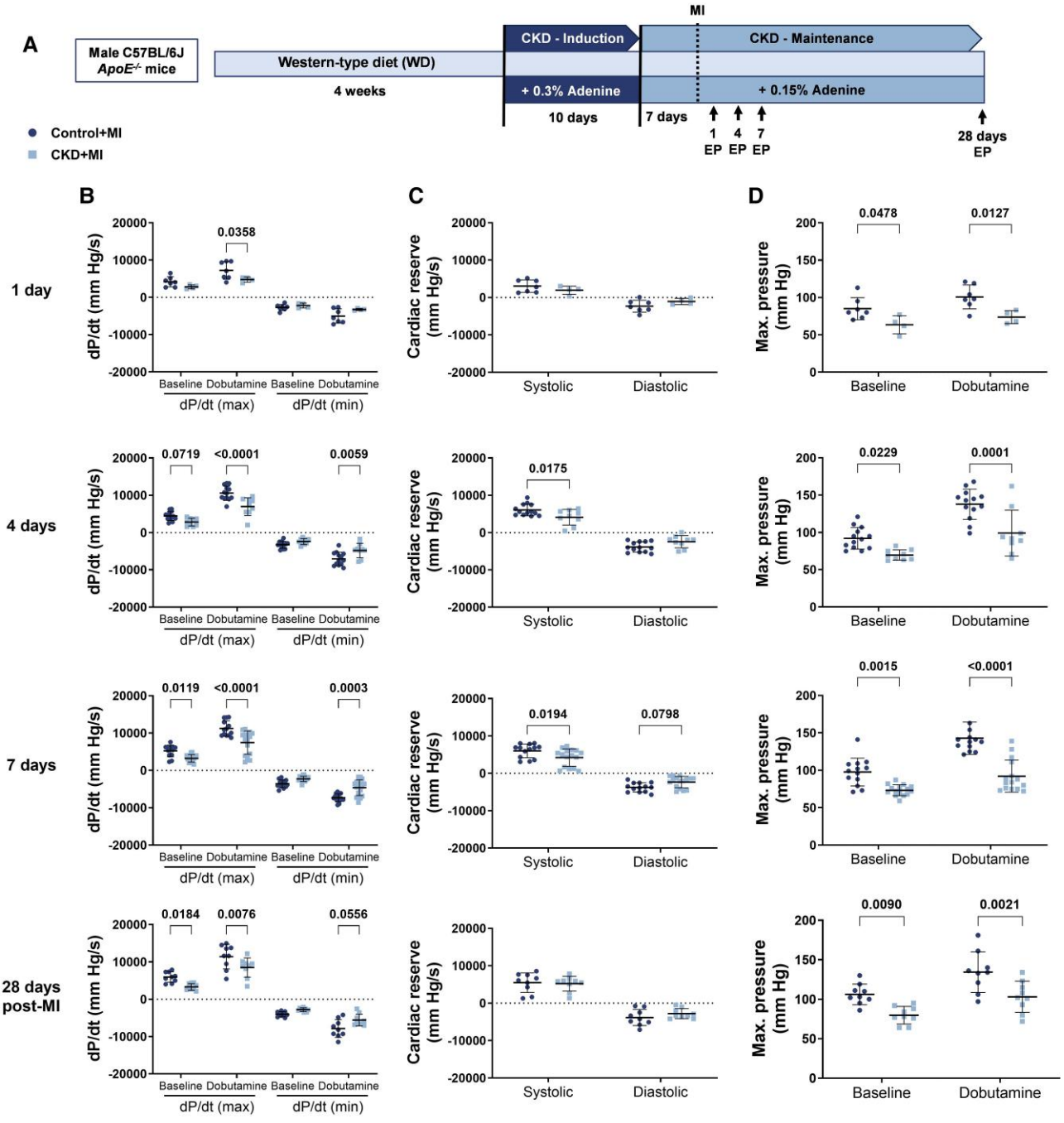

Figure 1 Murine CKD increases cardiac dysfunction after myocardial infarction. CKD was induced in male hyperlipidemic C57BL/6J *ApoE*$^{-/-}$ mice, followed by myocardial infarction (MI). Hyperlipidemic *ApoE*$^{-/-}$ mice without CKD as controls were similarly subjected to MI. (*A*) Experimental timeline. MI = myocardial infarction, WD = western-type diet, CKD = chronic kidney disease, EP = endpoint (for four separate experimental groups). (*B*–*D*) Invasive heart function analysis at day 1 (n = 3–7), 4 (n = 9–13), 7 (n = 13–16), or 28 (n = 9) post-MI by Millar catheter: (*B*) Maximal contractility ((dP/dT)max) and relaxation capacity ((dP/dT)min); (*C*) Cardiac reserve as delta (dP/dt) between dobutamine and baseline conditions; (*D*) Maximal left ventricular pressure. Shown are dot plots with means. Two-way ANOVA with Sidak's post-test for comparing CKD + MI mice to control + MI. For max. pressure 7 days post-MI (in *D*), one CKD mouse was excluded based on the Grubbs outlier test.

conditions 4–7 days post-MI (*Figure 1C*). Deterioration of relaxation ability—indicated by minimal dP/dT—started four days post-MI in stressed conditions (*Figure 1C*). In addition, maximal LV pressure was decreased over four weeks post-MI in CKD compared to non-CKD mice, both in resting conditions as well as upon dobutamine-induced stress (*Figure 1D*). Blood pressure remained unchanged (see Supplementary material online, *Figure S2B*).

In summary, post-MI, CKD significantly aggravated systolic and diastolic dysfunction at rest and stress conditions compared to non-CKD mice.

3.2 CKD increases circulating myeloid cell numbers post-MI

Cardiac infarction size remained unaffected between the groups despite increased cardiac dysfunction post-MI in CKD compared to non-CKD mice (see Supplementary material online, *Figure S3A–B*). Also, in the infarcted area, no differences were observed in the amount of apoptotic or proliferating cells nor in myofibroblast content, whereas the number of $CD31^+$ cells was increased in CKD mice (see Supplementary material online, *Figure S3C–F*). Post-MI blood profiling revealed in CKD mice an increased number of circulating monocytes and neutrophils compared to non-CKD mice, as well as an augmented percentage of neutrophils expressing CD54, which mediates pro-inflammatory neutrophil effector functions[25] (*Figure 2A* and *B*, Supplementary material online, *Figure S4A–B*). A slight increase was also observed in CCR1 expression on neutrophils in CKD vs. non-CKD mice post-MI (see Supplementary material online, *Figure S4A–C*), with CCR1 mediating neutrophil recruitment and detrimental inflammatory remodeling post-MI.[26]

We previously demonstrated that the chemokines CCL6 and CCL9 as important regulators of CCR1-mediated neutrophil and

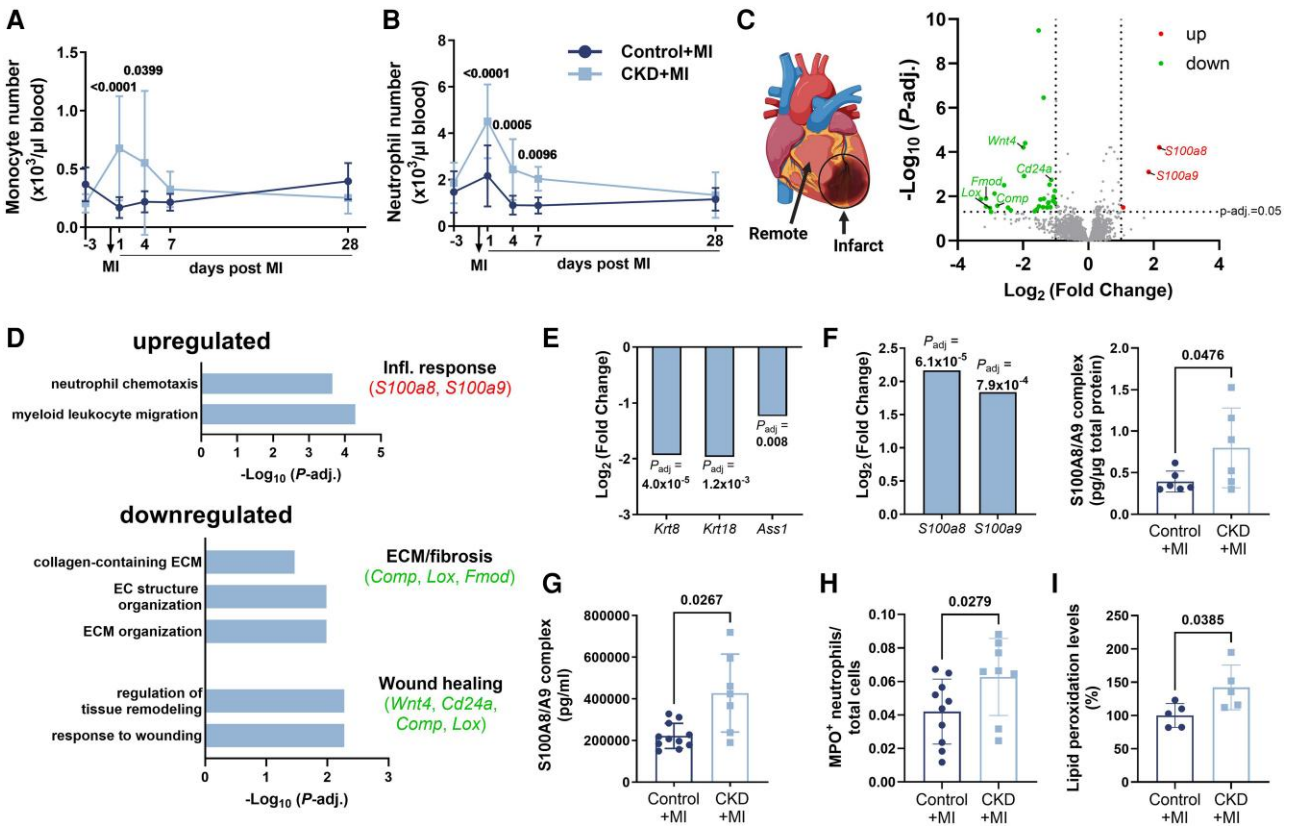

Figure 2 Murine CKD increases circulating monocyte and neutrophil numbers post-infarction, and up-regulates S100A8/A9, neutrophils, and lipid peroxidation stress in the infarcted heart. Hyperlipidemic *ApoE*$^{-/-}$ mice without vs. with CKD were subjected to MI. Time of analysis: one week post-MI, unless differently indicated. (*A–B*) Number of monocytes and neutrophils (CD45+ CD11b+ CD115− Gr1+) in blood before and at different time points after MI. Means ± SD. n = 6–7 (−3 days), n = 12–13 (1 day), n = 8–15 (4 days), n = 12–16 (7 days), and n = 8–11 (28 days). *Outlier exclusion based on the Grubbs outlier test (A: one non-CKD mouse 7 days post-MI; B: one CKD mouse 7 days post-MI, one CKD and one non-CKD mouse 28 days post-MI).* (*C*) RNAseq analysis of remote left ventricular (LV) tissue of the infarcted heart, as displayed. The Volcano plot depicts $\log_2$(Fold change) and $-\log_{10}(P_{adjusted})$ of gene expression comparing the CKD to non-CKD mice. Differentially expressed genes (DEGs) with $P_{adjusted} < 0.05$ and $\log_2$(Fold change) > 1 or <−1 are displayed on the right (up-regulated) or on the left side (down-regulated) of the plot. S100A8 and S100A9 are highlighted. (*D*) Representation of enriched gene ontology (GO) terms based on the significant DEGs, displaying down-regulated and up-regulated processes. Selected significant DEGs associated with these GO terms are indicated. (*E*) Gene expression of Keratin 8 (*Krt8*), Keratin 18 (*Krt18*), and argininosuccinate synthetase 1 (*Ass1*) in remote LV tissue of the infarcted heart, comparing CKD to non-CKD mice. Derived from RNAseq (n = 6–8). (*F*) S100A8 and S100A9 expression in remote LV tissue of the infarcted heart, comparing CKD to non-CKD mice. Left panel: On gene level as derived from RNAseq (n = 6–8). Right panel: S100A8/A9 protein complex as determined by ELISA (n = 6/group; Mean ± SD). (*G*) S100A8/A9 protein complex in serum one day post-MI as determined by ELISA (Mean ± SD; n = 7–11). (*H*) Myeloperoxidase $(MPO)^+$ cells in the remote LV tissue of the infarcted heart four days post-MI (Mean ± SD; n = 8–10). (*I*) Lipid peroxidation level in remote cardiac LV tissue, normalized to protein content and displayed relative to 'Control + MI'. (Mean ± SD; n = 5/group). *Tissue from CKD vs. non-CKD mice 7 days post-MI (both with isotype antibody treatment as in* Supplementary material online, Figure *S5C).* (A–B, F–I) Two-way ANOVA with Sidak's post-test (*A*,*B*), one-tailed Student t-test with (*F*) or without (*H*) Welch correction, or two-tailed Student t-test with (*I*) or without (*G*) Welch correction for comparing CKD + MI to control + MI mice.

monocyte recruitment are up-regulated in early experimental CKD.[27] Consistent with these findings, the present study shows that circulating levels of both chemokines were elevated in CKD mice compared with controls, both in the absence and presence of MI (see Supplementary material online, *Figure S5A–B*). However, blocking of either CCL6 or CCL9 failed to reverse the CKD-associated impairment in cardiac function following MI (see Supplementary material online, *Figure S5C–D*, *Table S2*).

3.3 CKD increases neutrophils, alarmins S100A8/A9, and lipid peroxidation stress in the infarcted heart

Next, we performed a multi-omics screening on infarcted and remote cardiac LV tissues of both groups to identify potential mechanisms underlying the increased cardiac dysfunction observed in post-MI CKD mice. Screening was conducted on 7 days post-MI samples representing an intermediate state between acute inflammation and chronic remodeling post-infarction. RNAseq revealed increased expression of genes involved in processes of heart contraction, oxidative stress, and mitochondrial function, and a simultaneous downregulation of genes coding for processes of extracellular matrix organization and wound healing in the infarcted cardiac tissue of CKD compared to non-CKD mice (see Supplementary material online, *Figure S6A*). Alterations were also observed in genes involved in calcium signaling, cardiac electrical function, and cardiac energy processes (see Supplementary material online, *Figure S6B–C*). A downregulation of genes involved in processes of extracellular matrix organization and wound healing in CKD conditions was also observed in cardiac LV tissue remote from the infarcted region (*Figure 2C* and *D*). For example, CKD significantly down-regulated gene expression of Keratin 8 and 18 (*Figure 2E*), which were both previously reported to increase in the infarcted heart to provide cardioprotection and support cardiac contractile function of the infarcted heart.[28]

Furthermore, this remote cardiac LV tissue—but not the infarcted region itself—displayed a significant upregulation of the alarmins S100A8 and S100A9 in CKD conditions (*Figure 2F*-left, Supplementary material online, *Figure S7*). The latter could be further confirmed for the S100A8/A9 heterodimer on the protein level (*Figure 2F*, right). In addition, levels of the S100A8/A9 complex were also increased in blood of CKD compared to control mice post-MI (*Figure 2G*). Complementary to S100A8/A9, its receptors Toll-like receptor-4 (TLR-4) and RAGE were also expressed in the remote LV region of the infarcted heart, without differences between CKD vs. non-CKD conditions [TLR4: $\log_2(FC) = -0.16$; $P_{adj} = 0.77$; RAGE: $\log_2(FC) = -0.41$; $P_{adj} = 0.68$].

Data within the Human Protein Atlas revealed these alarmins to be expressed mainly by myeloid cells (neutrophils but also macrophages) in the heart[29,30] (see Supplementary material online, *Figure S8*). In our mouse model, the total number of monocytes, macrophages, and neutrophils in the infarcted region or the overall heart tissue was not altered (see Supplementary material online, *Figure S3G–J*). However, neutrophils were detected in the remote LV region of the infarcted heart, where they were enriched in CKD compared to non-CKD conditions (*Figure 2H*). Also, lipid peroxidation levels as a readout of oxidative stress were significantly increased in the remote LV region of the infarcted heart in CKD vs. non-CKD animals (*Figure 2I*), without differences observed in lipid peroxidation amount in the absence of infarction (see Supplementary material online, *Figure S9*). CKD mice also displayed a reduced expression of argininosuccinate synthetase 1 (*Ass1*) in the remote LV tissue of the infarcted heart (*Figure 2E*), an enzyme that was recently shown to counteract lipid peroxidation in cancer cells.[31]

In summary, CKD increases neutrophils, the alarmins S100A8/A9, and lipid peroxidation stress in the infarcted heart.

3.4 CKD increases NR4A1 phosphorylation and MAP kinase activation in the infarcted heart

Complementary to our RNAseq analysis, unbiased multiplex kinome activity profiling of cardiac protein extracts derived from remote LV tissue 7 days post-MI revealed increased kinase activity in CKD mice. Specifically, downstream phosphorylation of the peptide GRRGRLPSKPKQP was significantly higher in CKD compared with non-CKD animals (*Figure 3A*). Protein blast exposed that this peptide uniquely belonged to the transcription factor orphan nuclear receptor 4A1 (NR4A1; AA 347-359), with S^{354} being a main NR4A1 serine phosphorylation site in mouse.[32] In line, additional mass spectrometry analysis confirmed the presence of significantly higher levels of NR4A1 phosphorylation at S^{354} (peptide LPS*KPK; with S* phosphorylated) in protein lysate from remote LV tissue in infarcted CKD compared to infarcted non-CKD mice (*Figure 3B*). Beyond NR4A1, only the NR4A1 family members NR4A2 and NR4A3 also contain the amino acid sequence LPSKPK as confirmed by protein blast. However, both NR4A2 and NR4A3 were overall very low expressed in LV remote tissue of the infarcted heart based on their RNAseq transcript levels and on average around 10–20 times lower than NR4A1 (*Figure 3C*), underlining NR4A1 as the main phosphorylated target quantified by mass spectrometry.

NR4A1 is a transcription factor activated downstream of S100A9.[33] Reanalyzing previously published single-nucleus RNAseq data of human healthy and infarcted hearts,[24] we validated cardiac NR4A1 expression, with cardiomyocytes as the main cell type expressing NR4A1 (*Figure 3D*). In our mouse model, CKD conditions did not alter NR4A1 on a transcript level in remote LV tissue (*Figure 3C*). Nonetheless, NR4A1 has previously been linked to stress-induced cardiomyocyte dysfunction through phosphorylation-dependent translocation from the nucleus to the mitochondria,[34,35] making it an attractive pathophysiological target.

Among 82 kinases identified as having an increased activity in cardiac tissue from CKD vs. non-CKD mice (see Supplementary material online, *Table S3*), 27 were predicted kinases for NR4A1. Ranking these kinases by their average RNAseq-derived expression in the remote cardiac LV tissue revealed PKA, AKT, and p38 in the top 7 of highest expressed kinases (*Figure 3E*). Notably, p38 kinase (MAPK14) is known to induce NR4A1 phosphorylation[36] and promotes its cytoplasmic localization,[37] while PKA, PKC, AKT, and RSK1/2 are known to directly interact with and phosphorylate S^{354} of NR4A1.[35,38] Increased abundance of phosphorylated (active) p38 in remote LV tissue of CKD compared to non-CKD mice was confirmed by western blot analysis (*Figure 3F*).

In summary, CKD increases p38 kinase activation and the phosphorylation of the NR4A1 as a detrimental event in cardiomyocyte function.

3.5 Elevated S100A8/S100A9 in CKD patients post-infarction as well as in the injured human heart

Analyzing circulating levels of the protein complex S100A8/A9 in patients revealed a slight increase in patients with early CKD [CKD3, 30 ≤ estimated glomerular filtration rate (eGFR) < 60] and a significant upregulation in more advanced stages of kidney dysfunction (CKD4/5, eGFR<30) (*Figure 4A* and *B*). Overall, circulating levels of S100A8/A9 increased after acute MI, with significantly higher post-infarction levels of S100A8/A9 in patients with kidney dysfunction (eGFR<60) compared to those without (eGFR≥60) (*Figure 4C*). Also, analyzing S100A8 and S100A9 expression

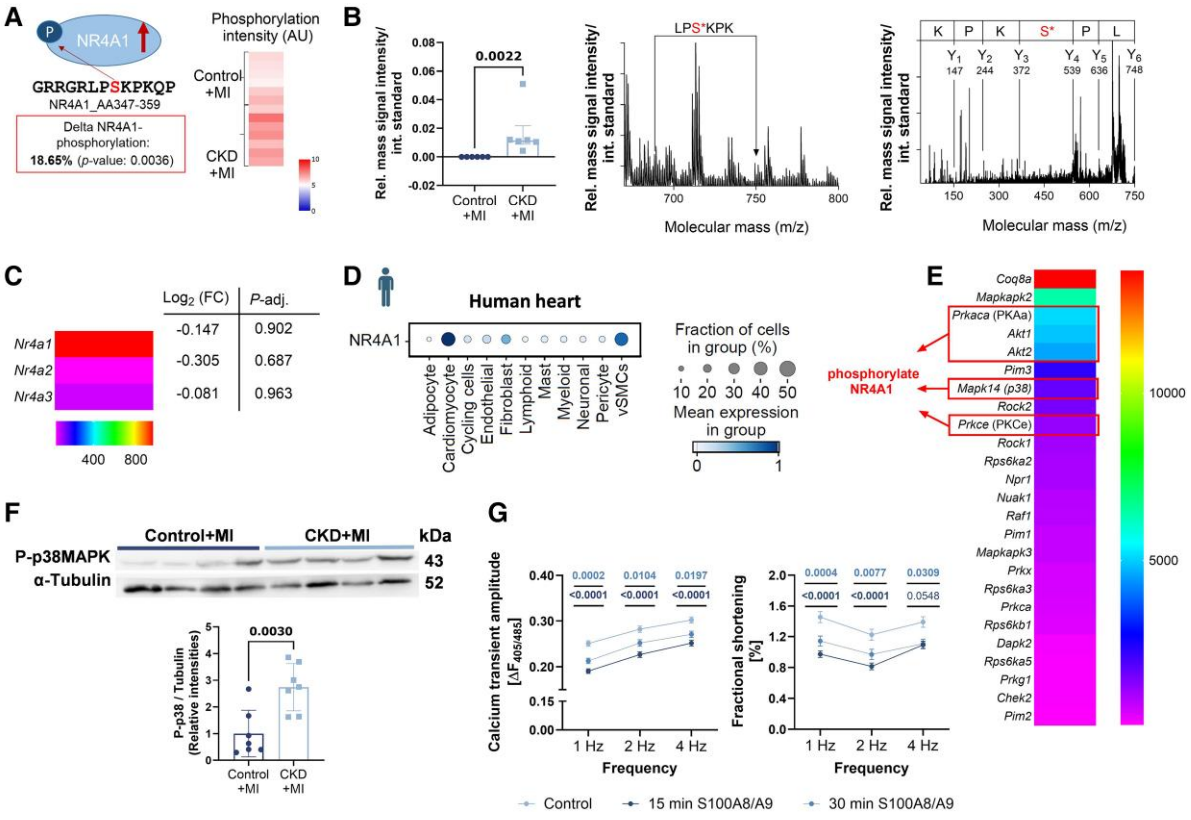

Figure 3 Murine CKD increases cardiac p38 kinase activation and NR4A1 phosphorylation post-infarction, and S100A8/A9 can directly trigger cardiomyocyte dysfunction. (A–C, F–G) Hyperlipidemic *ApoE*$^{-/-}$ mice without vs. with CKD were subjected to MI. Time of analysis: one week post-MI. (*A*) Increased phosphorylation of NR4A1 peptide by cardiac protein extracts of remote left ventricular (LV) tissue, comparing infarcted CKD to infarcted non-CKD mice in a kinase activity array. $n = 7–8$. With heat map. (*B*) Increased phosphorylation of NR4A1 (peptide LPS*KPK; with S* phosphorylated) quantified by mass spectrometry in protein lysates of remote cardiac LV tissue, comparing infarcted CKD to infarcted non-CKD mice, with quantification relative to internal standard (Mean ± SD; $n = 6$; Two-tailed Mann–Whitney test) and representative MS and MS/MS spectrum in CKD + MI mice. (*C*) Heatmap of average expression ('BaseMean') of *NR4A1*, *NR4A2*, and *NR4A3* transcripts in remote LV tissue of the infarcted heart via RNAseq data, with inclusion of Fold Change (FC) and adjusted *P*-value comparing CKD vs. non-CKD mice ($n = 6–8$). (*D*) Expression of NR4A1 in the human heart, as derived from single-nucleus RNA-Seq data of human infarcted heart and healthy controls[24]: Shown is cardiac expression of NR4A1 on the tissue level over the different cell types and conditions including infarcted and control hearts reflecting both cell-intrinsic expression and the abundance of cells expressing those genes in the given cell types. (*E*) Selection strategy of activated kinases in the remote LV cardiac tissue post-MI in relation to NR4A1 S^{351} phosphorylation: Starting from kinases predicted to be increasingly activated in CKD conditions and able to phosphorylate NR4A1 by the kinase activity array (*27, with 2 not displayed due to too low expression via RNAseq)*, 10 kinases had a high average expression in remote cardiac tissue ('BaseMean' > 1000) via RNAseq, of which 5 (in the highlighted box) have been validated in the literature to trigger the phosphorylation of NR4A1. (*F*) Western blot for phosphorylated p38 MAPK (P-p38) in remote cardiac LV tissue normalized to α-Tubulin as control, and displayed relative to the 'Control + MI' group (Means ± SD; $n = 7$; two-tailed Student *t*-test). Representative western blot shown. *One high value in each group excluded based on Grubb's test.* (*G*) Primary cardiomyocytes from C57BL/6J mice were stimulated *ex vivo* with S100A8/A9 (1 µg/mL) for 15 or 30 min, as indicated. Cardiomyocytes displayed a reduced calcium transient amplitude and a reduced fractional sarcomere shortening upon stimulation with S100A8/A9; N = 167–225 cells (from 3 mice); Means ± SEM. Kruskal–Wallis test with Dunn's multiple comparisons test for comparison of stimulated cells to control cells.

patterns in the human heart using available single-nucleus RNAseq data[24] showed myeloid cells as predominant cell type expressing S100A8 and S100A9 (*Figure 4D–F*). The overall myeloid-derived S100A8 and S100A9 expression was higher in the cardiac region remote from the infarcted area compared to control hearts (*Figure 4G*, Supplementary material online, *Figure S8C–D*), the latter being in line with the findings in our mouse model.

In summary, in human, post-MI levels of S100A8 and S100A9 are increased in blood of CKD compared to non-CKD patients and in the infarcted heart mainly myeloid cell-derived (*Figure 4H*).

3.6 Impairment of cardiomyocyte calcium handling and contraction capacity upon acute exposure to S100A8/A9 *ex vivo*, but no *in vivo* pharmacological targeting of S100A8/A9 detected that supports cardiac function post-infarction

S100A8/A9 treatment has previously been linked to reduced cardiac performance in the post-ischemic heart in mice and also

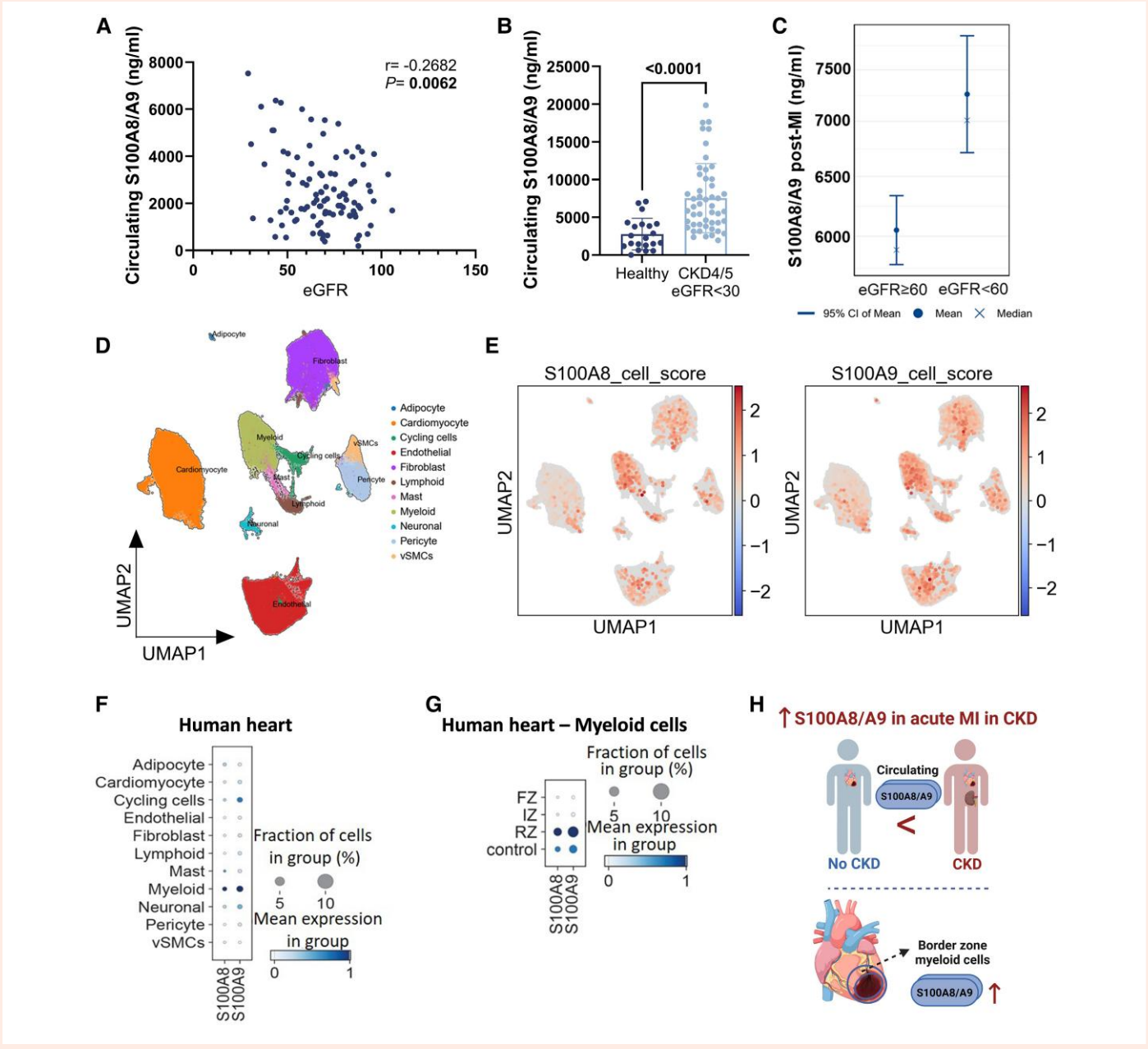

Figure 4 Elevated S100A8/S100A9 in CKD patients post-infarction as well as in the remote zone of the infarcted human heart. (*A*–*B*) Circulating levels of the S100A8/A9 protein complex in patients with CKD compared to healthy controls or patients without kidney dysfunction (eGFR≥60), as indicated. Measured by ELISA. (*A*) Cohort: Patients from the HF-PROTECT study (serum). Correlation between eGFR and circulating S100A8/9 levels. Pearson correlation coefficient (two-tailed): r = –0.2682, *P* = 0.0062, and N = 103. (*B*) Cohort: Healthy controls (N = 21) vs. patients with kidney dysfunction in stage CKD4 or CKD5 (eGFR<30; N = 49) (serum). Two-tailed Mann–Whitney test. (*C*) Circulating S100A8/A9 levels in patients with acute myocardial infarction, comparing patients with eGFR<60 (kidney dysfunction) vs. those with eGFR≥60. N = 1390 (serum). Shown are means + 95% CI; median indicated by 'x'. For eGFR≥60: N = 1043; For eGFR<60: N = 347. Unpaired two-tailed *t*-test; *P* = 0.000092. (*D*–*G*) Expression of S100A8 and S100A9 in the human heart, as derived from single-nucleus RNA-Seq data of human infarcted heart and healthy controls.[24] (*D*) UMAP visualization of snRNA-Seq data, with cell cluster identification as previously described.[24] (*E*) Cardiac expression of S100A8 and S100A9 (over the different conditions of infarcted and control hearts). (*F*) Cardiac expression of S100A8 and S100A9 on tissue level over the different cell types and conditions including infarcted and control hearts reflecting both cell-intrinsic expression and the abundance of cells expressing those genes in the given cell types. (*G*) Comparison of myeloid cell expression of S100A8 and S100A9 in control hearts (control) or the infarcted heart with either the necrotic area (ischemic zone, IZ) or the unaffected left ventricular myocardium (remote zone, RZ). The fibrotic zone (FZ) is derived from human heart specimens at later stages (>30 days) post-myocardial infarction. (*H*) *Summary scheme of human perspective:* Compared to non-CKD patients, CKD patients display increased circulating levels of S100A8/A9 post-infarction. Also, expression of S100A8 and S100A9 is increased in the infarcted human heart compared to a healthy heart, with both alarmins mainly originating from myeloid cells in the border zone remote from the infarcted area. *eGFR, estimated glomerular filtration rate.*

activated in this context the p38 kinase,[39] which itself was shown to be able to impact on cardiomyocyte Ca^{2+} handling.[40] Therefore, we next investigated a potential direct impact of the S100A8/A9 protein complex on cardiomyocyte function (using 1 µg/mL, in the range of values in blood of CKD mice, *Figure 2F*). Primary cardiomyocytes isolated from C57BL/6J mice were paced with a frequency from 1 to 4 Hz and analyzed for intracellular Ca^{2+} concentrations and sarcomere length. This revealed a disturbance in Ca^{2+} levels in both diastole and systole and a reduced calcium transient amplitude upon prior stimulation with S100A8/A9, along with reduced fractional sarcomere shortening (*Figure 3G*, Supplementary material online, *Figure S10*). The mitochondrial redox state and the dynamic range of the mitochondrial membrane potential in primary cardiomyocytes were not affected by short-term S100A8/A9 stimulation *ex vivo* (see Supplementary material online, *Figure S11*). Also, the intrinsic respiration capacity of mitochondria in the heart post-infarction was not affected by CKD: when comparing CKD to non-CKD mice; no significant overall difference was observed in the oxygen consumption rate of mitochondria isolated from the border zone of the infarcted area 7 days post-MI, nor from a non-infarcted heart under similar CKD vs. non-CKD conditions, in contrast to a reduced mitochondrial respiration rate in kidney upon CKD induction (see Supplementary material online, *Figure S12*).

We next investigated whether the detrimental effect of acute S100A8/A9 exposure triggering cardiomyocyte dysfunction as observed *ex vivo* could be translated into an overall cardioprotective effect *in vivo* by treating hyperlipidemic *ApoE*$^{-/-}$ mice with an S100A8/A9 inhibitor along with MI induction. Complementary to cardiac functional analysis, we also analyzed potential effects on circulating neutrophil counts, based on a previous study showing an improved cardiac function post-MI in an *S100A9*-knockout mouse model that was mechanistically linked to reduced MI-induced granulopoiesis and reduced blood neutrophils counts post-MI.[41] However, in contrast to *S100A9*-deficiency,[41] short-term *in vivo* pharmacological intervention using Paquinimod or ABR-238901 did not reduce peripheral blood neutrophil counts nor improve cardiac function post-MI (see Supplementary material online, *Figure S13*).

In summary, systemic S100A8/A9 levels are elevated in CKD patients, and acute exposure of cardiomyocytes to S100A8/A9 *ex vivo* disrupts calcium handling and cardiomyocyte contractile function without eliciting intrinsic mitochondrial stress. However, since no short-term *in vivo* pharmacological intervention targeting the S100A8/A9 complex has been identified that improves cardiac function post-MI, our findings provide a rationale for further investigation into downstream cardiac alterations that may contribute to the aggravated cardiac dysfunction post-MI in CKD.

3.7 CKD disturbs cellular metabolism in the infarcted heart, with metabolic alterations associated with poorer cardiac performance post-MI

Since metabolic changes significantly impact cardiac function post-MI,[10,11] we next performed untargeted metabolomics analysis with pathway analysis on cardiac LV tissue 7 days post-MI in CKD vs. non-CKD conditions. This revealed alterations in the metabolism of glycerophospholipids in the infarcted area (see Supplementary material online, *Figure S14A*). Also, the remote LV region presented altered glycerophospholipid metabolism in addition to changes in galactose metabolism (*Figure 5A*, Supplementary material online, *Figure S14B*). Focusing on molecular alterations in the remote region, 165 of a total of 1917 identified metabolite peaks were found to be significantly changed when comparing CKD to non-CKD mice after infarction, with the top 25 metabolites ranked by significance displayed in a heatmap (*Figure 5B*). This revealed that pantothenic acid—a precursor of the important energy metabolite Coenzyme A (CoA)—was significantly up-regulated in CKD mice and presented in the top 5 of altered metabolites (see Supplementary material online, *Table S4*). Similarly, pantothenic acid appeared in the top 5 of overall 46 significantly altered metabolites in the infarcted area (see Supplementary material online, *Table S4*). An independent targeted metabolomics analysis of the remote LV region with focus on cellular energy metabolism pathways confirmed the upregulation of pantothenic acid in CKD context (*Figure 5C*). In parallel, a decrease in the levels of CoA and CoA-conjugated fatty acids (acetyl-CoA, propionyl-CoA) was detected (*Figure 5C*), suggesting a disturbed conversion of pantothenic acid to CoA and a subsequently decreased availability of CoA-conjugated fatty acids.

The conversion of pantothenic acid to CoA involves the enzymes PANK1-4, PPCS, PPCDC, and COASY (see Supplementary material online, *Figure S15A*), with the first step catalyzed by PANK enzymes as the rate-limiting step. Among the PANK enzymes with the classical pantothenate kinase activity (PANK1-3), *Pank1* was the highest expressed in the infarcted heart in our mouse model (see Supplementary material online, *Figure S15B*). This was also observed in the human infarcted heart, with cardiomyocytes being the main cellular source of cardiac *PANK1* expression based on a re-analysis of available single-nucleus RNAseq data[24] (see Supplementary material online, *Figure S15C*). However, none of the PANK enzymes was altered on the RNA level in the remote LV region of the infarcted heart when comparing CKD to non-CKD mice, as obvious from our RNAseq data [$\log_2$(FC) (P_{adj}) for *Pank1*: 0.08 (0.92); *Pank2* (0.97): 0.01; *Pank3*: 0.05 (0.88); and *Pank4*: 0.13 (0.79)] (see Supplementary material online, *Figure S15B*). Also, *Ppcs*, *Ppcdc*, and *Coasy* gene expression was not altered (see Supplementary material online, *Figure S15B*). PANK1 expression in the remote LV region of the infarcted heart was not altered by CKD on the protein level either (see Supplementary material online, *Figure S15D–G*).

In addition to altered pantothenic acid-CoA metabolism, CKD mice showed increased levels of hexose/inositol (which includes mainly glucose) in the remote area of the infarcted heart (*Figure 5D*), despite reduced glucose levels in the blood, especially in conditions of infarction (see Supplementary material online, *Figure S14C*). Cardiac levels of glycerol-3-phosphate (Gro3P) were reduced in CKD mice, which is indicative for a disturbed Gro3P shuttle downstream of glycolysis (*Figure 5D*). While expression of the glucose receptors GLUT1 (*Slc2a1*) and GLUT4 (*Slc2a4*) was not altered as evident from the RNAseq analysis, CKD mice displayed a reduced cardiac expression of glucokinase (*Gck*) (*Figure 5E*). GCK encodes hexokinase-IV, an enzyme which can trigger the first step of glycolysis.

Given these important metabolic alterations in the heart (*Figure 5F*), we next investigated a potential correlation with cardiac function parameters. Of note, a strong positive linear correlation was detected between CoA levels and cardiac performance (cardiac contraction, relaxation capacity, and maximal pressure), whereas substrate precursors pantothenic acid and hexose/inositol both showed an inverse correlation with cardiac performance (*Table 1*, *Figure 5G*, Supplementary material online, *Figure S16*). Increased pantothenic acid and reduced CoA were also detected in the heart upon the mere induction of CKD without additional MI, however, for CoA less pronounced compared to post-MI conditions and without significant reductions in acetyl-CoA (see Supplementary material online, *Figure S14D*), a key substrate for the citric acid cycle toward ATP production. Furthermore, CKD alone did not significantly affect cardiac levels of hexose/inositol or glycerol-3-phosphate (see Supplementary material online, *Figure S14D*).

Combined, these findings indicate that CKD disturbs cardiac cellular metabolism post-MI: CKD triggers a signature of impaired glycolysis, reduced levels of CoA and acetyl-CoA as well as a disturbed

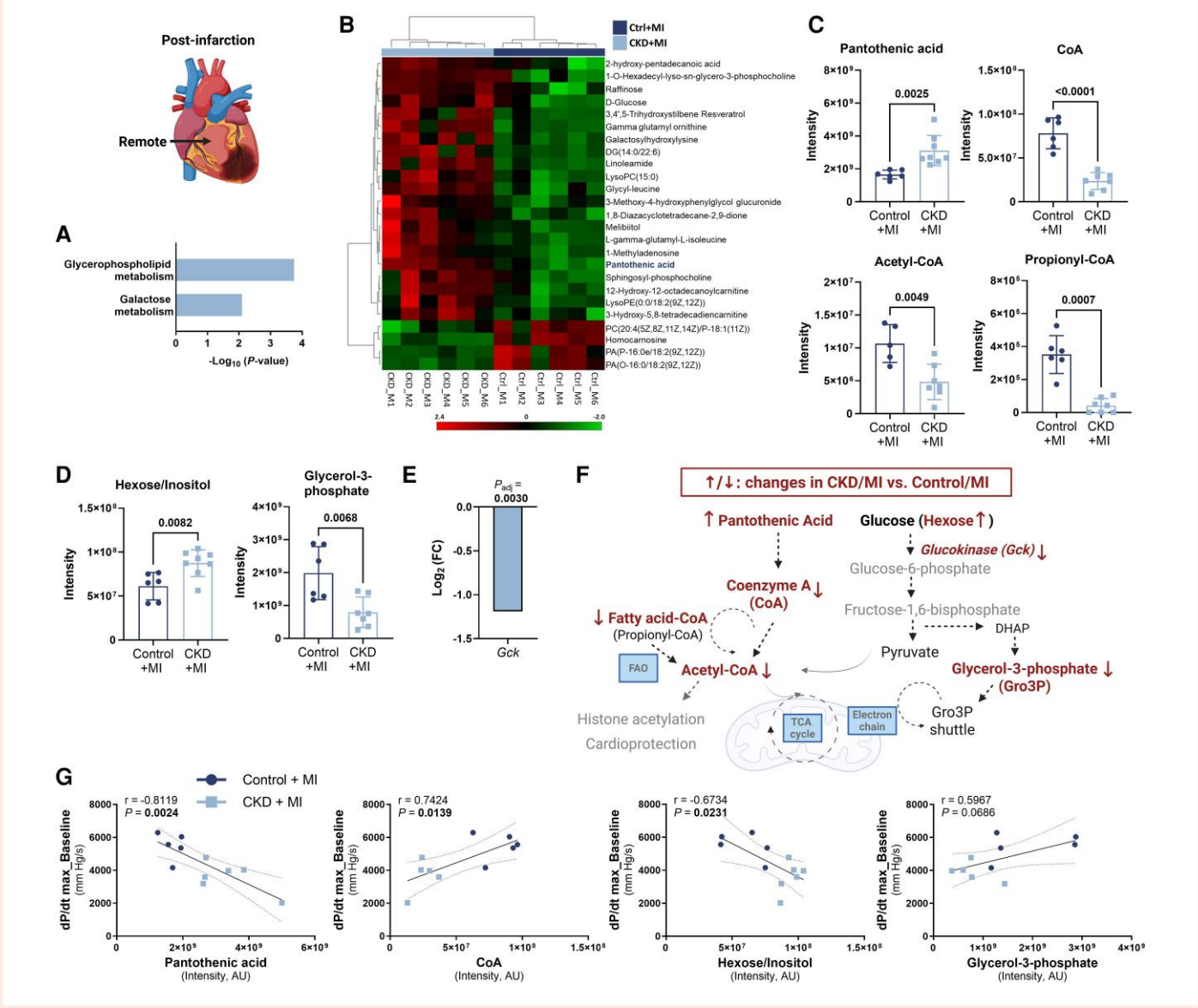

Figure 5 CKD alters the cellular metabolism in the murine heart post-infarction. Hyperlipidemic *ApoE*$^{-/-}$ mice without vs. with CKD were subjected to MI, with molecular analysis performed 7 days post-MI. Analysis was performed on the remote LV tissue of the infarcted heart. (*A*–*B*) Untargeted metabolomics, with (*A*) pathway analysis and (*B*) heatmap of the top 25 metabolites (when ranked by significance). (*C*–*D*) Targeted metabolomics, with intensity normalized to tissue weight (arbitrary units). Shown is mean ± SD. *n* = 5–8. Outlier exclusion based on Grubbs outlier test. Two-tailed Student *t*-test with or without Welch correction for comparing CKD + MI to control + MI mice. (*E*) *Gck* expression on gene level, derived from RNAseq (*n* = 6–8). *FC, fold change.* (*F*) Summary of metabolic changes in relation to glycolysis, fatty acid oxidation (FAO), and the citric acid cycle (TCA cycle) post-infarction in CKD vs. non-CKD mice. *DHAP, dihydroxyacetonephosphate.* (*G*) Correlation analysis of metabolites in the cardiac tissue with cardiac performance parameters (dP/dT)max. r, Pearson correlation coefficient; with linear regression fit and 95% confidence interval. N = 6/group with both Millar and metabolomics data available; one outlier was excluded in CKD group for CoA and Gro3P based on the Grubbs outlier test.

Gro3P shuttle downstream of glycolysis (summarized in *Figure 5F*), with these alterations associated with poorer cardiac performance post-MI.

4. Discussion

Triggered by the increased hospitalization rate and mortality of CKD patients following MI,[8,42] this study investigated the impact of CKD on the infarcted heart. Our data indicate that CKD increases systemic inflammation post-infarction with a higher number of circulating myeloid cells (monocytes and neutrophils). Furthermore, in CKD, the infarcted heart displayed a signature of increased inflammation and oxidative stress, disturbances in contraction and calcium signaling pathways as well as in cellular energy metabolism. The latter was associated with poorer cardiac performance post-MI in CKD compared to non-CKD conditions (*Figure 6*).

No cardiac dysfunction was detected in the absence of MI in our CKD mouse model, as we previously reported for this mouse model.[19] However, in this study, CKD did aggravate cardiac

Table 1 Correlation analysis between cardiac metabolites and cardiac performance

Cardiac metabolites vs. function	*dP/dt max _Baseline (mm Hg/s)*	*dP/dt max _Dobutamine (mm Hg/s)*	*dP/dT min _Baseline (mm Hg/s)*	*dP/dT min _Dobutamine (mm Hg/s)*	*Pmax _Baseline (mm Hg)*	*Pmax _Dobutamine (mm Hg)*
Pantothenic acid	*r = –0.8119*	*r = –0.5282*	*r = 0.7033*	*r = 0.74*	*r = –0.751*	*r = –0.8391*
(Intensity, AU)	*P =* ***0.0024***	*P = 0.0949*	*P =* ***0.0158***	*P =* ***0.0092***	*P =* ***0.0077***	*P =* ***0.0012***
CoA	*r = 0.7424*	*r = 0.4097*	*r = –0.6736*	*r = –0.438*	*r = 0.6739*	*r = 0.7003*
(Intensity, AU)	*P =* ***0.0139***	*P = 0.2397*	*P =* ***0.0327***	*P = 0.2054*	*P =* ***0.0326***	*P =* ***0.0241***
Hexose	*r = –0.6734*	*r = –0.4599*	*r = 0.7886*	*r = 0.3422*	*r = –0.7357*	*r = –0.5109*
(Intensity, AU)	*P =* ***0.0231***	*P = 0.1547*	*P =* ***0.0039***	*P = 0.303*	*P =* ***0.0099***	*P = 0.1083*
Glycerol-3-phosphate	*r = 0.5967*	*r = 0.2071*	*r = –0.6914*	*r = –0.1121*	*r = 0.6647*	*r = 0.3414*
(Intensity, AU)	*P = 0.0686*	*P = 0.566*	*P =* ***0.0268***	*P = 0.7578*	*P =* ***0.036***	*P = 0.3343*

Mouse model as in *Figure 1A*, comparing non-CKD vs. CKD mice 7 days post-myocardial infarction. Cardiac parameters analyzed in baseline or upon dobutamine stress. Metabolites analyzed in the remote left ventricular tissue of the infarcted heart. Shown are correlation analyses between cardiac metabolites and cardiac performance, with r, Pearson correlation coefficient, and associated *P*-value. Significant correlations are highlighted ($0.7 \leq r$ (very strong positive correlation); $0.5 \leq r < 0.7$ (strong positive correlation); $r \leq -0.7$ (very strong negative correlation); $-0.7 < r \leq -0.5$ (strong negative correlation)). *N = 6/group with both Millar and metabolomics data available; one outlier excluded in CKD group for CoA and Gro3P based on Grubbs outlier test.* For visualization, see *Figure 5G* and Supplementary material online, *Figure S16*. *AU, arbitrary units.*

dysfunction of the infarcted heart in both resting conditions as well as upon cardiac stress, with also a minor but significant decrease in the cardiac contractile reserve. This was not due to a difference in the infarction size, which we demonstrated to be equal in CKD vs. non-CKD conditions, as could also be expected in a MI model with permanent ligation. Furthermore, cardiac myofibroblast content in the infarcted area was unaltered, suggesting an impact of CKD on alternative processes, such as inflammation and cardiomyocyte functionality. MI-induced rises in circulating monocyte and neutrophil numbers were enhanced in CKD conditions in mice, which in patients with acute MI is a strong, independent predictor of left ventricular dysfunction, hospitalization, and death.[43,44] Furthermore, in the CKD model, circulating neutrophils showed an increased surface expression of CD54 and also accumulated to a higher extent in cardiac LV tissue remotely of the infarcted region. Inflammation-induced expression of CD54—also known as ICAM1—on neutrophils is linked to an increased pro-inflammatory phenotype with enhanced ROS production.[25]

In parallel to an increased number of myeloid cells in the circulation and an enhanced neutrophil accumulation in cardiac LV tissue remotely of the infarcted region, the remote LV region showed increased levels of lipid peroxidation stress as well as of the alarmin complex S100A8/A9, enhanced p38 MAP kinase activation, and increased phosphorylation of NR4A1 shortly after infarction (*Figure 6*), all of which have been linked to cardiomyocyte damage and cardiac dysfunction after ischemia.[35,40,41,45–50] MAP kinase p38 signaling has previously been linked to cardiac inflammation, injury, and dysfunction.[47,48] P38 also has a direct anti-inotropic effect on the heart by altering the phosphorylation status of contractile proteins as well as by impacting on cardiomyocyte Ca^{2+} handling by regulating—for example—the expression and/or activity of the sarcoplasmic/endoplasmic reticulum Ca^{2+}-ATPase 2 (SERCA2).[40] Furthermore, S100A9 is able to increase NR4A1 expression and activity,[33] and an increased NR4A1 expression as well as a translocation from nuclear to cytosolic and mitochondrial localization have previously been observed in cardiomyocytes in the border zone of ischemic myocardium as well as in stressed cardiomyocytes, through which NR4A1 prompted pro-apoptotic responses.[35,49] Also, NR4A1 is up-regulated in the heart following transverse aortic constriction and dysregulates calcium flux homeostasis in cardiomyocytes.[50] Although our RNAseq analysis did not reveal an altered expression of NR4A1 in CKD compared to non-CKD mice, we did detect increased Ser^{354} phosphorylation of NR4A1 in the remote LV area of the infarcted heart in CKD, with also NR4A1 Ser^{354} phosphorylation previously implicated in stress-induced cardiomyocyte dysfunction.[35] In parallel, analysis of the post-infarcted heart of CKD compared to non-CKD mice revealed increased kinase activity of p38, PKA, and AKT, all of which can phosphorylate NR4A1.[35] PKA-induced phosphorylation of NR4A1 at Ser^{351} (the human phosphorylation site equivalent to Ser^{354} in mice) was shown to trigger its translocation from the nucleus to the mitochondria and thereby induce cardiomyocyte apoptosis.[34,35] Combined, along with aggravated cardiac dysfunction post-infarction in CKD compared to non-CKD conditions, our study identified increased neutrophil numbers, oxidative stress, and inflammation as well as altered molecular signaling in the infarcted heart in CKD, all previously linked to cardiomyocyte dysfunction.

The pro-inflammatory proteins S100A8 and S100A9 are mainly secreted from myeloid cells, including in the heart,[29,30] and predominantly form S100A8/A9 heterodimers.[51] Our further investigations into cardiac S100A8 and S100A9 expression showed an increased myeloid cell-derived S100A8 and S100A9 expression in the remote zone of human cardiac tissue post-MI compared to healthy heart. Furthermore, our data revealed higher circulating S100A8/A9 levels in CKD patients compared to controls, and even after acute MI, these S100A8/A9 levels were maintained at increased levels in patients with kidney dysfunction, similarly as observed in our CKD mouse model. In animal models, short-term pharmacological intervention of S100A8/A9 signaling with ABR-238901 post-MI has been shown to induce protein expression changes potentially indicative of improved cardiac contractility[52] and to stimulate cardiac neovascularization[53] and reduce oxidative stress.[54] In our study, we identified a direct detrimental effect of the S100A8/A9 heterodimer toward disturbances in contractile responses and calcium flux in primary cardiomyocytes *ex vivo*, with the underlying mechanisms currently still unclear. However, in three dose-finding experiments *in vivo*, we could not identify a short-term treatment regime with Paquinimod or ABR-238901 that provided a beneficial effect on cardiac contractile or relaxation function post-MI. Paquinimod (ABR-215757) and ABR-238901 both belong to the quinoline-3-carboxamide class and function as an inhibitor of the S100A8/A9 heterodimer (and of S100A9) by blocking the interaction of S100A9 with both RAGE and TLR4.[46,55] Potentially, unaffected S100A8-governed signaling or S100A8/A9 signaling over alternative binding routes, with, e.g. binding to heparan sulfate proteoglycans and

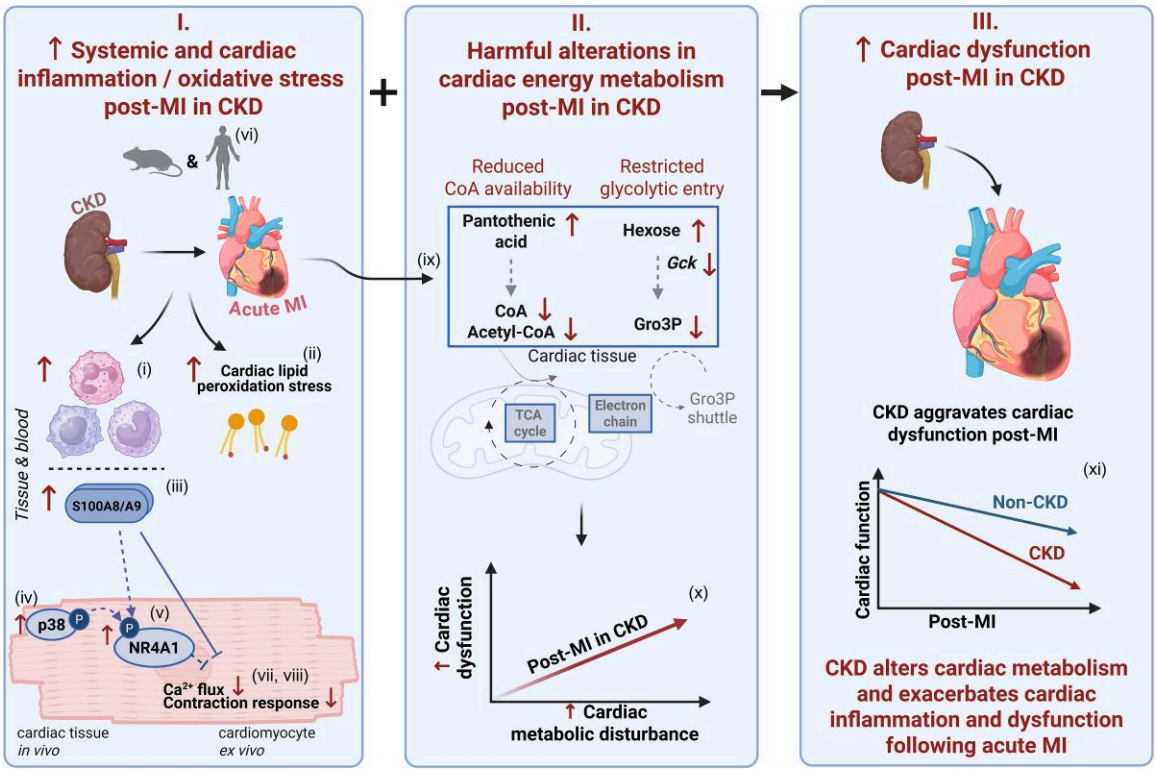

Figure 6 CKD increases cardiac oxidative stress and inflammation including S100A8/A9 release, triggers harmful alterations in cardiac energy metabolism, and aggravates cardiac dysfunction post-infarction. (*I*) Compared to non-CKD mice, CKD demonstrated an increased systemic and cardiac inflammation and oxidative stress post-MI: CKD increased the number of circulating myeloid cells (neutrophils and monocytes) into the blood post-MI as well as the accumulation of neutrophils in the cardiac LV tissue remote from the infarcted region (i). In parallel, CKD increased lipid peroxidation stress in the infarcted heart (ii) and triggered a stronger accumulation of the myeloid-derived acute stress proteins S100A8 and S100A9 in circulation as well as in the remote zone of the infarcted heart (iii). Also, CKD enhanced p38-phosphorylation (iv) and Ser^{354}-phosphorylation of NR4A1 (v) in the remote cardiac LV tissue, with both p38[35] and S100A9[33] known to trigger NR4A1 phosphorylation and/or activation. NR4A1 and NR4A1 Ser^{354}-phosphorylation have previously been implicated in stress-induced cardiomyocyte dysfunction.[35,49,50] Of note, single-nucleus RNAseq data revealed also increased expression of S100A8 and S100A9 in the infarcted human heart compared to healthy controls, with both alarmins mainly originating from myeloid cells in the border zone remote from the infarcted area (vi). In addition, increased circulating levels of S100A8/A9 shortly after an acute MI could be detected in patients with kidney dysfunction (eGFR<60) compared to those without (eGFR≥60) (vi). Furthermore, the S100A8/A9 complex exerted an acute detrimental impact on calcium flux (vii) and contractile responses (viii) in primary cardiomyocytes, as shown *ex vivo*, although without a benefit of a short-term pharmacological intervention on cardiac function post-MI identified *in vivo*. (II) In parallel, CKD triggered harmful alterations in cellular energy metabolism in the heart post-MI with a restricted glycolytic entry, a reduced glycerol-3-phosphate (Gro3P) shuttle, and a shortage of the cellular energy metabolite Coenzyme A in CKD vs. non-CKD mice post-MI (ix), with these alterations associated with poorer cardiac performance post-MI (x). (III) Combined, these changes in inflammation, oxidative stress and cardiac metabolic changes were associated with aggravated cardiac dysfunction post-MI in CKD compared to non-CKD mice (xi). *CKD, chronic kidney disease; CoA, coenzyme A; Gck, glucokinase; Gro3P, glycerol-3-phosphate; and MI, myocardial infarction. Created with BioRender.com.*

carboxylated glycans on endothelial cells shown,[51] may underlay the absence of *in vivo* effects of Paquinimod or ABR-238901. Alternatively, other danger-associated molecules or their receptors may compensate for the loss of S100A8/A9 signaling upon acute pharmacological blockade *in vivo*. Also in previous studies, the *in vivo* impact of pharmacologically targeting S100A8/A9 signaling on cardiac function post-MI suffered from experimental variability: both an improved[46] as well as a neutral[54] effect on cardiac function post-MI were reported among studies using a similar short-term S100A8/A9 targeting strategy involving ABR-238901 (3 days-treatment of C57BL/6 mice, each 30 mg/kg/day *i.p.* starting on the day of MI induction, analyzed 3 days[54] or 7–21 days[46] post-MI). Two other studies investigating an identical treatment with ABR-238901 reported only on effects on cardiac remodeling post-MI but not cardiac function.[52,53] Of note, prolonged S100A9 blockade is contraindicated: detrimental effects of daily ABR-238901 treatment were observed already 7 days post-MI, triggering a progressive deterioration of cardiac function post-MI due to a dual function of S100A9 in inflammation and repair.[33] In summary, although the S100A8/A9 heterodimer exerts direct negative effects on calcium handling and contraction in cardiomyocytes *ex vivo* as shown in our study, systemic *in vivo* targeting in our mouse model does not seem to offer a straightforward strategy to reproducibly improve cardiac function post-MI. Nonetheless, in patients, high S100A8/A9 levels post-infarction have been shown to be associated with an increased risk of major adverse cardiovascular events including rehospitalization for heart failure and death.[46,56] Thus, our findings of increased post-MI plasma levels

of S100A8/A9 in CKD compared to non-CKD patients could still indicate a potential poorer outcome for this patient group post-infarction, warranting a follow-up validation study.

Beyond increased cardiac inflammation and oxidative stress, CKD mice also showed metabolic alterations in the cardiac LV area remotely to the infarction zone, with a disturbed conversion of pantothenic acid to CoA and a downstream decreased availability of CoA-conjugated fatty acids, in addition to increased hexose levels but reduced levels of Gro3P (*Figure 6*). These characteristics may each contribute to cardiac dysfunction: CoA and acetyl-CoA—the latter produced both by glycolysis and the oxidation of fatty acids (*Figure 6*)—are key metabolites for cellular energy production, and their limited availability as we detected in CKD conditions post-MI may compromise cardiac energy supply. The heart highly depends for energy on fatty acid oxidation—which requires CoA-conjugated fatty acids in the mitochondria with production of acetyl-CoA—and compromised fatty acid oxidation is a main characteristic of heart failure.[57] Also, acetyl-CoA supports cardiac function post-MI/RI by mediating histone acetylation and thereby reducing cardiomyocyte oxidative stress.[58] The mechanisms underlying these metabolic alterations in CKD remain currently unclear. The PANK enzymes (mainly PANK1 in the heart) are the rate-limiting enzymes in the conversion of pantothenic acid to CoA, with additional key roles for PANK4 as a regulatory unit,[59] PPCS, PPCDC, and COASY (see Supplementary material online, *Figure S15A*). Our data indicate that CKD does not induce gene expression changes for any of these enzymes in the infarcted heart and also does not alter PANK1 on a protein level. However, it remains to be investigated whether CKD affects cardiac metabolites in the infarcted heart by dysregulating the functional activity of these enzymes, e.g. triggered by the detected increased cardiac peroxidation levels post-infarction in CKD conditions. Post-translational modifications have indeed been increasingly acknowledged to alter protein function and associated pathophysiological processes and cardiovascular risk in CKD.[60]

In addition to reduced levels of CoA and acetyl-CoA, also the reduced levels of Gro3P—as observed in the cardiac LV area remotely to the infarction zone in CKD compared to non-CKD mice—may negatively impact on the heart. Gro3P is known to reduce mitochondrial stress through the Gro3P shuttle, which regenerates cytosolic NAD^+ by transferring electrons from cytosolic NADH to the electron transfer chain in the mitochondrial matrix.[61] Of note, Gro3P is a side product of glycolysis and can be produced from fructose 1,6-bisphosphate—a main intermediate of glycolysis—over dihydroxyacetone phosphate (DHAP).[62] Increased glucose levels in the absence of increased GLUT1/GLUT4 expression in combination with reduced levels of acetyl-CoA and Gro3P point to disturbances in glycolysis, whereas the latter was shown to be cardioprotective post-infarction.[63] Our observation of the CKD-associated reduction of the glucokinase GCK in the infarcted heart may contribute to dysregulation of glycolysis and associated metabolic branch points. GCK belongs to the group of hexokinases, which mediate the first step of glycolysis. Although family members hexokinase 1 and 2 are higher expressed in the myocardium compared to GCK, a loss of cardioprotection was revealed after ischemia/reperfusion injury and oxygen deprivation stress by downregulation of GCK, with GCK shown to promote glycolysis and thereby support cardiomyocyte survival.[64]

Overall, the observed cardiac metabolic alterations post-MI in CKD vs. non-CKD conditions were associated with poorer cardiac performance. Compared to ischemic conditions, less pronounced CKD-induced downregulation of CoA in the absence of MI, as well as unaltered cardiac levels of acetyl-CoA, hexose, and Gro3P in CKD vs. non-CKD mice in the absence of MI may explain the absence of cardiac dysfunction upon CKD induction without MI, in contrast to the observed aggravated cardiac dysfunction post-MI in CKD vs. non-CKD mice. Furthermore, the overall mitochondrial respiration capacity of isolated cardiac mitochondria was not affected by CKD in ischemic or non-ischemic conditions. Taken together, our findings indicate that the metabolic changes observed in murine remote LV tissue in CKD vs. non-CKD mice post-MI (accumulation of pantothenic acid with depletion of CoA and acetyl-CoAs, together with increased hexose, reduced GCK expression, and decreased Gro3P) do not result from an intrinsic defect in mitochondrial respiratory capacity, but rather from CKD-associated impairment in post-MI metabolic adaptation in the remote LV, characterized by restricted glycolytic entry and a functional limitation in (acyl-)CoA bioavailability. This reduced metabolic input in the ischemic heart in CKD conditions could predispose the heart to an aggravated cardiac dysfunction post-MI, potentially in combination with pro-oxidative alterations as we observed in the heart. Hence, rather than suppressing innate immune-associated responses such as S100A8/A9 with double-edged functions in cardiac remodeling, targeting both cardiomyocyte intrinsic oxidative and metabolic stress, such as p38/NR4A1 activation combined with CoA-dependent metabolic limitations, may provide support for the ischemic heart in CKD conditions.

As limitation, our permanent ligation myocardial infarction model reflects the clinical scenario of patients with acute STEMI without fast, successful reperfusion, but not the scenario of fast revascularization, which is better reflected in the myocardial ischemia–reperfusion injury model. Furthermore, the adenine-induced CKD model involves crystal deposition in kidney tissue, which rapidly impairs kidney function and induces inflammation with pronounced tubulointerstitial fibrosis. While this model is extensively used to examine the cardiorenal axis, it differs from the more gradual loss of kidney function in human CKD. Also, since the adenine-induced CKD model shows sex differences in CKD development,[65] we included only male mice in this study to exclude differential effects on the infarcted heart merely due to different degrees in kidney damage between sexes. A follow-up study in female mice remains recommended. Finally, other CKD models than those used in this study (using different mouse strains, CKD induction methods, and/or CKD duration) could observe cardiac remodeling and cardiac functional changes upon solely CKD induction.[12–18] This is expected to further impact cardiac remodeling post-infarction, with the extent to be further examined in a follow-up study.

In conclusion, our study reveals for the first time that CKD increases innate immune activation, inflammation, and oxidative stress in the infarcted heart as well as triggers cardiac metabolic alterations characterized by restricted glycolytic entry and a functional limitation in (acetyl-)CoA bioavailability. This is accompanied by an aggravated cardiac dysfunction post-infarction in CKD compared to non-CKD conditions, independent of infarct size, with poorer cardiac performance in CKD associated with the cardiac metabolic alterations (*Figure 6*). Combined, these changes may contribute to the poorer outcome of CKD patients post-infarction compared to patients with healthy kidney function. Future studies should examine whether S100A8/A9 has a value as predictive biomarker for poorer cardiovascular outcome post-infarction in CKD patients, as recently shown for post-MI heart failure in the general population.[66] Also, further studies are required into how precisely CKD affects cardiac energy metabolism and whether this forms a potential therapeutic target. With CKD strongly impacting on cell pathways through post-translational modifications of proteins,[60] the question arises whether CKD may trigger detrimental post-translational modifications of key enzymes within metabolic pathways, and whether modulation of the activity of these enzymes (e.g. PANK) may provide cardioprotection post-MI in CKD conditions. In this context, SGLT2 inhibitors emerge as particularly interesting, especially considering preclinical evidence suggesting an off-target activation of PANK1 as a likely contributor to their cardioprotective effects.[67]

Translational perspective

Patients with chronic kidney disease (CKD) exhibit a reduced survival following myocardial infarction. We discovered that CKD triggers metabolic alterations in the infarcted heart, leading to reduced levels of energy-providing metabolites. Also, CKD increased inflammatory cells, acute phase proteins, and lipid peroxidation in the heart post-infarction, and activated molecular pathways linked to cardiomyocyte dysfunction. S100A8/A9 had a detrimental impact on cardiomyocytes and was also increased in CKD patients post-infarction. By revealing a detrimental axis of both inflammatory and metabolic changes, this study increases the understanding of aggravated cardiac dysfunction in CKD post-infarction and reveals novel targets for translational research.

Supplementary material

Supplementary material is available at *Cardiovascular Research* online.

Authors' contributions

Conceptualization, H.N. Methodology and experimentation: C.S., J.W., S.Hou., E.H., J.M., M.K., V.J., H.J., S.M., F.H., D.W.L.W., E.P.C.v.d.V., S.V., B.G., C.M., P.S.-K., L.P.-R., M.L., R.K., P.B., S.Ha., C.M., H.N. Provision of patient cohorts: M.B., B.K., M.B., E.G., H.A.K., S.S., D.F., K.M.-S., F.K. Data analysis: C.S., J.W., S.Hou., E.H., J.M., C.V.C.J., M.K., V.J., H.J., M.R., S.M., D.W.L.W., E.P.C.v.d.V., F.K., C.M., B.G., M.R., S.Ha., H.N. Discussion of results: E.A.L.B., U.S.-S., C.G., J.J., Y.D., C.M., N.M., H.N. Writing—original draft preparation: C.S., E.H., S.Hou., H.N. Writing—review and editing: All authors.

Acknowledgements

We thank Josefin Soppert for support with the animal application; Jenny Uhl and Shauni Loopmans for support with untargeted and targeted metabolomics, respectively; as well as Helen Demollin, Tim Schulz, Nadine Persigehl, Linus Meusel, Melanie Garbe, Steffi Elbin, Yuan Kong, and Roya Soltan for excellent technical support. Furthermore, this work was supported by the Flow Cytometry Facility, a core facility of the Interdisciplinary Center for Clinical Research (IZKF) Aachen within the Faculty of Medicine at RWTH Aachen University. We thank Heidi Deigentasch (Study Nurse, University Hospital Heidelberg) for helping to provide patient parameters from the biobank. Figures were in part created with Biorender.com.

Conflict of interest: B.K. has served as a speaker for Novo Nordisk, Lilly, SphingoTec, 4TEEN4 Pharmaceuticals, DGK-Akademie, and the Professional Association of German Internists (BDI e.V.), has consulted for Novo Nordisk and Roche Diagnostics and has received travel support from Novo Nordisk, Lilly, Boehringer Ingelheim, AstraZeneca, Apontis Pharma, Daiichi Sankyo, Edwards Lifesciences, Medtronic, 4TEEN4 Pharmaceuticals, the German Society of Lipidology, DGK-Akademie and the German Cardiac Society. F.K. has served as a speaker for Novo Nordisk, Boehringer Ingelheim, Bayer, Amgen, Apontis Pharma, Eli Lilly, AstraZeneca, C.T.I., Cogitando, Synlab, CSL Vifor, DGK-Akademie, SphingoTec, 4TEEN4 Pharmaceuticals and diaplan GmbH, consulted Novo Nordisk, Eli Lilly, Bayer, Apontis Pharma, Pricewaterhouse Coopers/Strategy&, and received travel support from Amgen, Novo Nordisk, Boehringer Ingelheim, Bayer, SphingoTec, 4TEEN4 Pharmaceuticals, diaplan GmbH, C.T.I., Cogitando, and Eli Lilly. S.Ha. is a co-founder of Sequantrix GmbH and reports research funding from Novo Nordisk and Askbio. R.K. is a founder, shareholder, and board member of Sequantrix GmbH; is a member of the scientific advisory board of Hybridize Therapeutics; has received honoraria for advisory boards and talks from Bayer, Chugai, Pfizer, Roche, Genentech, Eli Lilly, AMGEN, Novo Nordisk, Valerio Therapeutics, and GlaxoSmithKline; and has research funding from Travere Therapeutics, Galapagos, Novo Nordisk, and AskBio. C.M. received honoraria for advisory boards and talks from AstraZeneca, Boehringer Ingelheim, Bristol Myers Squibb, Cytokinetics, Lilly, and Novo Nordisk. The other authors report that no conflict of interest exists.

Funding

This research was supported by the German Research Foundation (DFG SFB/TRR219 Project-ID 322900939 to V.J., E.v.d.V., C.G., L.P.R., S.S., D.F., K.M.S., M.L., F.K., J.J., R.K., P.B., N.M., and H.N.; DFG SFB1382 Project-ID 403224013 to H.N. and J.J.); DFG SFB1739 (to V.J., E.v.d.V., U.S.-S., K.M.S., J.J., R.K., P.B., N.M., and H.N.); and the European Union's Horizon 2020 research and innovation program under the Marie Skłodowska-Curie Grant Agreement No. 764474 (CaReSyAn, to H.N., J.J., and E.B.). Additional support was provided by the Else Kröner-Fresenius-Stiftung (Project 2020_EKEA.60 to H.N.), the Interdisciplinary Centre for Clinical Research within the faculty of Medicine at the RWTH Aachen University (1-12 to H.N.), the START Program of the Faculty of Medicine of the RWTH Aachen University (112/22 to C.S.; 011/24 to J.W.); and the German Centre for Cardiovascular Research (DZHK-B23Ex to H.N.). The study was also supported by EFSD and Boehringer Ingelheim European Research Programme on "Multi-System Challenges in Diabetes, Obesity and Cardiometabolic Disease" 2024 to H.N. C.V.C.J. was supported by the Alexander von Humboldt Foundation (post-doctoral fellowship) and the RWTH Start-Up Project (StUpPD_436-23). E.P.C.v.d.V. was further supported by a grant from the Interdisciplinary Center for Clinical Research within the faculty of Medicine at the RWTH Aachen University and by the Corona Foundation (S199/10084/2021). P.B. was supported by the German Research Foundation (DFG Project-ID 454024652, 432698239, and 445703531), the European Research Council (ERC; Consolidator Grant AIM.imaging. CKD, No. 101001791), and the Federal Ministry of Education and Research (BMBF, STOP-FSGS-01GM1901A). C.M. received support by DFG SFB 1525 (project ID 453989101), Ma 2528/8-1 (project ID 505805397), and 9-2 (project ID 315254108). K.M.-S. was further supported by a grant from the Interdisciplinary Centre for Clinical Research within the Faculty of Medicine at the RWTH Aachen University (IZKF OC2-4). B.K. was supported by the Clinician Scientist Program of the Faculty of Medicine RWTH Aachen University. F.K. was funded by the German Research Foundation (DFG, 520275106, Emmy Noether Research Group; SFB TRR 219; Project-ID 322900939 [M-07]), the European Research Area Network on Cardiovascular Diseases and Federal Ministry of Education and Research (ERA-CVD and BMBF, Grant No. JTC-2019, MyPenPath—01KL2004), the European Foundation

for the Study of Diabetes (EFSD)/Novo Nordisk Foundation (NNF2OSA0066111), and the Interdisciplinary Centre for Clinical Research within the faculty of Medicine at the RWTH Aachen University (IZKF project PTD 1-11). S.Ha. was partially funded by the START Program of the Faculty of Medicine of the RWTH Aachen University and CRU344. J.M. received funding from Ernst und Berta Grimke Stiftung (9/22). B.G. received funding from the FWO (I012220N). U.S.-S. was funded by the German Federal Ministry of Education and Research (BMBF: 01EC1901B, Project 2).

Data availability

Data are included in the article and supplementary tables (see Supplementary material online, *Table S3*-Serine-Threonine Kinase Score Table as Excel file). Bulk RNA sequencing data of infarct and remote cardiac tissue 7 days post-MI, comparing CKD vs. non-CKD mice, are deposited in the Gene Expression Omnibus (GEO) database (GSE283464). Human single-nucleus (sn)-RNAseq data of human infarcted heart were previously published.[24] Processed snRNA-seq are available at the Zenodo data archive (https://zenodo.org/record/6578047). Additional experimental data supporting the findings of this study are available from the corresponding author upon reasonable request.

References

1. Hill NR, Fatoba ST, Oke JL, Hirst JA, O'Callaghan CA, Lasserson DS, Hobbs FD. Global prevalence of chronic kidney disease—a systematic review and meta-analysis. *PLoS One* 2016;**11**:e0158765.
2. Francis A, Harhay MN, Ong ACM, Tummalapalli SL, Ortiz A, Fogo AB, Fliser D, Roy-Chaudhury P, Fontana M, Nangaku M, Wanner C, Malik C, Hradsky A, Adu D, Bavanandan S, Cusumano A, Sola L, Ulasi I, Jha V; American Society of Nephrology; European Renal Association; International Society of Nephrology. Chronic kidney disease and the global public health agenda: an international consensus. *Nat Rev Nephrol* 2024;**20**:473–485.
3. Thompson S, James M, Wiebe N, Hemmelgarn B, Manns B, Klarenbach S, Tonelli M. Cause of death in patients with reduced kidney function. *J Am Soc Nephrol* 2015;**26**:2504–2511.
4. Matsushita K, Ballew SH, Wang AY, Kalyesubula R, Schaeffner E, Agarwal R. Epidemiology and risk of cardiovascular disease in populations with chronic kidney disease. *Nat Rev Nephrol* 2022;**18**:696–707.
5. Noels H, van der Vorst EPC, Rubin S, Emmett A, Marx N, Tomaszewski M, Jankowski J. Renal causes and consequences in the pathogenesis and progression of heart failure. *Circ Res* 2025;**136**:1306–1334.
6. Valdivielso JM, Rodríguez-Puyol D, Pascual J, Barrios C, Bermúdez-López M, Sánchez-Niño MD, Pérez-Fernández M, Ortiz A. Atherosclerosis in chronic kidney disease: more, less, or just different? *Arterioscler Thromb Vasc Biol* 2019;**39**:1938–1966.
7. Anavekar NS, McMurray JJ, Velazquez EJ, Solomon SD, Kober L, Rouleau JL, White HD, Nordlander R, Maggioni A, Dickstein K, Zelenkofske S, Leimberger JD, Califf RM, Pfeffer MA. Relation between renal dysfunction and cardiovascular outcomes after myocardial infarction. *N Engl J Med* 2004;**351**:1285–1295.
8. United States Renal Data System. *USRDS Annual Data Report: Epidemiology of Kidney Disease in the United States*. Bethesda, MD: National Institutes of Health, National Institute of Diabetes and Digestive and Kidney Diseases; 2021.
9. Frangogiannis NG. Regulation of the inflammatory response in cardiac repair. *Circ Res* 2012;**110**:159–173.
10. Peng X, Du J, Wang Y. Metabolic signatures in post-myocardial infarction heart failure, including insights into prediction, intervention, and prognosis. *Biomed Pharmacother* 2024;**170**:116079.
11. Zuurbier CJ, Bertrand L, Beauloye CR, Andreadou I, Ruiz-Meana M, Jespersen NR, Kula-Alwar D, Prag HA, Eric Botker H, Dambrova M, Montessuit C, Kaambre T, Liepinsh E, Brookes PS, Krieg T. Cardiac metabolism as a driver and therapeutic target of myocardial infarction. *J Cell Mol Med* 2020;**24**:5937–5954.
12. Soppert J, Frisch J, Wirth J, Hemmers C, Boor P, Kramann R, Vondenhoff S, Moellmann J, Lehrke M, Hohl M, van der Vorst EPC, Werner C, Speer T, Maack C, Marx N, Jankowski J, Roma LP, Noels H. A systematic review and meta-analysis of murine models of uremic cardiomyopathy. *Kidney Int* 2022;**101**:256–273.
13. Junho CVC, Frisch J, Soppert J, Wollenhaupt J, Noels H. Cardiomyopathy in chronic kidney disease: clinical features, biomarkers and the contribution of murine models in understanding pathophysiology. *Clin Kidney J* 2023;**16**:1786–1803.
14. Nemmar A, Al-Salam S, Beegam S, Zaaba NE, Yasin J, Hamadi N, Ali BH. Cardiac inflammation, oxidative stress, Nrf2 expression, and coagulation events in mice with experimental chronic kidney disease. *Oxid Med Cell Longev* 2021;**2021**:8845607.
15. Kaesler N, Cheng M, Nagai J, O'Sullivan J, Peisker F, Bindels EMJ, Babler A, Moellmann J, Droste P, Franciosa G, Dugourd A, Saez-Rodriguez J, Neuss S, Lehrke M, Boor P, Goettsch C, Olsen JV, Speer T, Lu TS, Lim K, Floege J, Denby L, Costa I, Kramann R. Mapping cardiac remodeling in chronic kidney disease. *Sci Adv* 2023;**9**:eadj4846.
16. Dargam V, Sanchez A, Kolengaden A, Perez Y, Arias R, Valentin Cabrera AM, Chaparro D, Tarafa C, Coba A, Yapaolo N, da Silva Nogueira P, Todd EA, Williams MM, Shehadeh LA, Hutcheson JD. Sex-specific changes in cardiac function and electrophysiology during progression of adenine-induced chronic kidney disease in mice. *J Cardiovasc Dev Dis* 2024;**11**:362.
17. Beikoghli Kalkhoran S, Basalay M, He Z, Golforoush P, Roper T, Caplin B, Salama AD, Davidson SM, Yellon DM. Investigating the cause of cardiovascular dysfunction in chronic kidney disease: capillary rarefaction and inflammation may contribute to detrimental cardiovascular outcomes. *Basic Res Cardiol* 2024;**119**:937–955.
18. Moellmann J, Glandien K, Klinkhammer BM, Wollenhaupt J, Noels H, Jankowski J, Lebherz C, Boor P, Lehrke M, Marx N. Development of a mouse model of uremic cardiomyopathy: investigating the impact of chronic kidney disease on cardiac function and signaling pathway. *Faseb J* 2025;**39**:e70639.
19. Wollenhaupt J, Frisch J, Harlacher E, Wong DWL, Jin H, Schulte C, Vondenhoff S, Moellmann J, Klinkhammer BM, Zhang L, Baleanu-Curaj A, Liehn EA, Speer T, Kazakov A, Werner C, van der Vorst EPC, Selejan SR, Hohl M, Böhm M, Kramann R, Biessen EAL, Lehrke M, Marx N, Jankowski J, Maack C, Boor P, Prates Roma L, Noels H. Pro-oxidative priming but maintained cardiac function in a broad spectrum of murine models of chronic kidney disease. *Redox Biol* 2022;**56**:102459.
20. Moellmann J, Krueger K, Wong DWL, Klinkhammer BM, Buhl EM, Dehairs J, Swinnen JV, Noels H, Jankowski J, Lebherz C, Boor P, Marx N, Lehrke M. 2,8-Dihydroxyadenine-induced nephropathy causes hexosylceramide accumulation with increased mTOR signaling, reduced levels of protective SirT3 expression and impaired renal mitochondrial function. *Biochim Biophys Acta Mol Basis Dis* 2024;**1870**:166825.
21. Kohlhaas M, Nickel AG, Bergem S, Casadei B, Laufs U, Maack C. Endogenous nitric oxide formation in cardiac myocytes does not control respiration during β-adrenergic stimulation. *J Physiol* 2017;**595**:3781–3798.
22. Nickel AG, Kohlhaas M, Bertero E, Wilhelm D, Wagner M, Sequeira V, Kreusser MM, Dewenter M, Kappl R, Hoth M, Dudek J, Backs J, Maack C. CaMKII does not control mitochondrial Ca(2+) uptake in cardiac myocytes. *J Physiol* 2020;**598**:1361–1376.
23. Nickel AG, von Hardenberg A, Hohl M, Löffler JR, Kohlhaas M, Becker J, Reil JC, Kazakov A, Bonnekoh J, Stadelmaier M, Puhl SL, Wagner M, Bogeski I, Cortassa S, Kappl R, Pasieka B, Lafontaine M, Lancaster CR, Blacker TS, Hall AR, Duchen MR, Kästner L, Lipp P, Zeller T, Müller C, Knopp A, Laufs U, Böhm M, Hoth M, Maack C. Reversal of mitochondrial transhydrogenase causes oxidative stress in heart failure. *Cell Metab* 2015;**22**:472–484.
24. Kuppe C, Ramirez Flores RO, Li Z, Hayat S, Levinson RT, Liao X, Hannani MT, Tanevski J, Wünnemann F, Nagai JS, Halder M, Schumacher D, Menzel S, Schäfer G, Hoeft K, Cheng M, Ziegler S, Zhang X, Peisker F, Kaesler N, Saritas T, Xu Y, Kassner A, Gummert J, Morshuis M, Amrute J, Veltrop RJA, Boor P, Klingel K, Van Laake LW, Vink A, Hoogenboezem RM, Bindels EMJ, Schurgers L, Sattler S, Schapiro D, Schneider RK, Lavine K, Milting H, Costa IG, Saez-Rodriguez J, Kramann R. Spatial multi-omic map of human myocardial infarction. *Nature* 2022;**608**:766–777.
25. Woodfin A, Beyrau M, Voisin MB, Ma B, Whiteford JR, Hordijk PL, Hogg N, Nourshargh S. ICAM-1-expressing neutrophils exhibit enhanced effector functions in murine models of endotoxemia. *Blood* 2016;**127**:898–907.
26. Liehn EA, Merx MW, Postea O, Becher S, Djalali-Talab Y, Shagdarsuren E, Kelm M, Zernecke A, Weber C. Ccr1 deficiency reduces inflammatory remodelling and preserves left ventricular function after myocardial infarction. *J Cell Mol Med* 2008;**12**:496–506.
27. Hemmers C, Schulte C, Wollenhaupt J, Wong DWL, Harlacher E, Orth-Alampour S, Klinkhammer BM, Schirmer SH, Böhm M, Marx N, Speer T, Boor P, Jankowski J, Noels H. Chemokine CCL9 is upregulated early in chronic kidney disease and counteracts kidney inflammation and fibrosis. *Biomedicines* 2022;**10**:420.
28. Papathanasiou S, Rickelt S, Soriano ME, Schips TG, Maier HJ, Davos CH, Varela A, Kaklamanis L, Mann DL, Capetanaki Y. Tumor necrosis factor-α confers cardioprotection through ectopic expression of keratins K8 and K18. *Nat Med* 2015;**21**:1076–1084.
29. Human Protein Atlas. **https://www.proteinatlas.org/ENSG00000143546-S100A8/single+cell/heart+muscle#tissue_cell_type (14 February 2025, date last accessed)**.
30. Human Protein Atlas. **https://www.proteinatlas.org/ENSG00000163220-S100A9/single+cell/heart+muscle (14 February 2025, date last accessed).**
31. Hu Q, Dai J, Zhang Z, Yu H, Zhang J, Zhu X, Qin Y, Zhang L, Zhang P. ASS1-Mediated reductive carboxylation of cytosolic glutamine confers ferroptosis resistance in cancer cells. *Cancer Res* 2023;**83**:1646–1665.
32. **www.phosphosite.org (26 March 2024, date last accessed).**

33. Marinković G, Koenis DS, de Camp L, Jablonowski R, Graber N, de Waard V, de Vries CJ, Goncalves I, Nilsson J, Jovinge S, Schiopu A. S100a9 links inflammation and repair in myocardial infarction. *Circ Res* 2020;**127**:664–676.
34. Hirata Y, Kiuchi K, Chen HC, Milbrandt J, Guroff G. The phosphorylation and DNA binding of the DNA-binding domain of the orphan nuclear receptor NGFI-B. *J Biol Chem* 1993;**268**:24808–24812.
35. Xinxing W, Hong F, Rui Z, Yun Z, Jingbo G, Lingjia Q. Phosphorylated nerve growth factor-induced clone B (NGFI-B) translocates from the nucleus to mitochondria of stressed rat cardiomyocytes and induces apoptosis. *Stress* 2012;**15**:545–553.
36. Yang HX, Sun JH, Yao TT, Li Y, Xu GR, Zhang C, Liu XC, Zhou WW, Song QH, Zhang Y, Li AY. Bellidifolin ameliorates isoprenaline-induced myocardial fibrosis by regulating TGF-β1/Smads and p38 signaling and preventing NR4A1 cytoplasmic localization. *Front Pharmacol* 2021;**12**:644886.
37. Kim HJ, Kim JY, Lee SJ, Kim HJ, Oh CJ, Choi YK, Lee HJ, Do JY, Kim SY, Kwon TK, Choi HS, Lee MO, Park IS, Park KG, Lee KU, Lee IK. α-Lipoic acid prevents neointimal hyperplasia via induction of p38 mitogen-activated protein kinase/Nur77-mediated apoptosis of vascular smooth muscle cells and accelerates post-injury reendothelialization. *Arterioscler Thromb Vasc Biol* 2010;**30**:2164–2172.
38. Kurakula K, Koenis DS, van Tiel CM, de Vries CJ. NR4A nuclear receptors are orphans but not lonesome. *Biochim Biophys Acta* 2014;**1843**:2543–2555.
39. Volz HC, Laohachewin D, Seidel C, Lasitschka F, Keilbach K, Wienbrandt AR, Andrassy J, Bierhaus A, Kaya Z, Katus HA, Andrassy M. S100a8/A9 aggravates post-ischemic heart failure through activation of RAGE-dependent NF-κB signaling. *Basic Res Cardiol* 2012;**107**:250.
40. Romero-Becerra R, Santamans AM, Folgueira C, Sabio G. P38 MAPK pathway in the heart: new insights in health and disease. *Int J Mol Sci* 2020;**21**:7412.
41. Sreejit G, Abdel-Latif A, Athmanathan B, Annabathula R, Dhyani A, Noothi SK, Quaife-Ryan GA, Al-Sharea A, Pernes G, Dragoljevic D, Lal H, Schroder K, Hanaoka BY, Raman C, Grant MB, Hudson JE, Smyth SS, Porrello ER, Murphy AJ, Nagareddy PR. Neutrophil-derived S100A8/A9 amplify granulopoiesis after myocardial infarction. *Circulation* 2020;**141**:1080–1094.
42. Yandrapalli S, Christy J, Malik A, Wats K, Harikrishnan P, Aronow W, Frishman W. Impact of acute and chronic kidney disease on heart failure hospitalizations after acute myocardial infarction. *Am J Cardiol* 2022;**165**:1–11.
43. Barron HV, Harr SD, Radford MJ, Wang Y, Krumholz HM. The association between white blood cell count and acute myocardial infarction mortality in patients > or =65 years of age: findings from the cooperative cardiovascular project. *J Am Coll Cardiol* 2001;**38**:1654–1661.
44. Maekawa Y, Anzai T, Yoshikawa T, Asakura Y, Takahashi T, Ishikawa S, Mitamura H, Ogawa S. Prognostic significance of peripheral monocytosis after reperfused acute myocardial infarction:a possible role for left ventricular remodeling. *J Am Coll Cardiol* 2002;**39**:241–246.
45. Cai Z, Xie Q, Hu T, Yao Q, Zhao J, Wu Q, Tang Q. S100a8/A9 in myocardial infarction: a promising biomarker and therapeutic target. *Front Cell Dev Biol* 2020;**8**:603902.
46. Marinković G, Grauen Larsen H, Yndigegn T, Szabo IA, Mares RG, de Camp L, Weiland M, Tomas L, Goncalves I, Nilsson J, Jovinge S, Schiopu A. Inhibition of pro-inflammatory myeloid cell responses by short-term S100A9 blockade improves cardiac function after myocardial infarction. *Eur Heart J* 2019;**40**:2713–2723.
47. Meldrum DR, Dinarello CA, Cleveland JC Jr, Cain BS, Shames BD, Meng X, Harken AH. Hydrogen peroxide induces tumor necrosis factor alpha-mediated cardiac injury by a P38 mitogen-activated protein kinase-dependent mechanism. *Surgery* 1998;**124**:291–296; discussion 297.
48. Kumphune S, Bassi R, Jacquet S, Sicard P, Clark JE, Verma S, Avkiran M, O'Keefe SJ, Marber MS. A chemical genetic approach reveals that p38alpha MAPK activation by diphosphorylation aggravates myocardial infarction and is prevented by the direct binding of SB203580. *J Biol Chem* 2010;**285**:2968–2975.
49. Cheng Z, Völkers M, Din S, Avitabile D, Khan M, Gude N, Mohsin S, Bo T, Truffa S, Alvarez R, Mason M, Fischer KM, Konstandin MH, Zhang XK, Heller Brown J, Sussman MA. Mitochondrial translocation of Nur77 mediates cardiomyocyte apoptosis. *Eur Heart J* 2011;**32**:2179–2188.
50. Medzikovic L, Schumacher CA, Verkerk AO, van Deel ED, Wolswinkel R, van der Made I, Bleeker N, Cakici D, van den Hoogenhof MM, Meggouh F, Creemers EE, Remme CA, Baartscheer A, de Winter RJ, de Vries CJ, Arkenbout EK, de Waard V. Orphan nuclear receptor Nur77 affects cardiomyocyte calcium homeostasis and adverse cardiac remodelling. *Sci Rep* 2015;**5**:15404.
51. Schiopu A, Cotoi OS. S100a8 and S100A9: DAMPs at the crossroads between innate immunity, traditional risk factors, and cardiovascular disease. *Mediators Inflamm* 2013;**2013**:828354.
52. Boteanu RM, Suica VI, Uyy E, Ivan L, Uta DV, Mares RG, Simionescu M, Schiopu A, Antohe F. Cardiac ATP production and contractility are favorably regulated by short-term S100A9 blockade after myocardial infarction. *J Adv Res* 2025;**77**:297–308.
53. Mares RG, Suica VI, Uyy E, Boteanu RM, Ivan L, Cocuz IG, Sabau AH, Yadav V, Szabo IA, Cotoi OS, Tomut ME, Jakobsson G, Simionescu M, Antohe F, Schiopu A. Short-term S100A8/A9 blockade promotes cardiac neovascularization after myocardial infarction. *J Cardiovasc Transl Res* 2024;**17**:1389–1399.
54. Vlad ML, Mares RG, Jakobsson G, Manea SA, Lazar AG, Preda MB, Popa MA, Simionescu M, Schiopu A, Manea A. Therapeutic S100A8/A9 inhibition reduces NADPH oxidase expression, reactive oxygen species production and NLRP3 inflammasome priming in the ischemic myocardium. *Eur J Pharmacol* 2025;**996**:177575.
55. Björk P, Björk A, Vogl T, Stenström M, Liberg D, Olsson A, Roth J, Ivars F, Leanderson T. Identification of human S100A9 as a novel target for treatment of autoimmune disease via binding to quinoline-3-carboxamides. *PLoS Biol* 2009;**7**:e97.
56. Li Y, Chen B, Yang X, Zhang C, Jiao Y, Li P, Liu Y, Li Z, Qiao B, Bond Lau W, Ma XL, Du J. S100a8/a9 signaling causes mitochondrial dysfunction and cardiomyocyte death in response to ischemic/reperfusion injury. *Circulation* 2019;**140**:751–764.
57. Bertero E, Maack C. Metabolic remodelling in heart failure. *Nat Rev Cardiol* 2018;**15**:457–470.
58. Lei I, Tian S, Gao W, Liu L, Guo Y, Tang P, Chen E, Wang Z. Acetyl-CoA production by specific metabolites promotes cardiac repair after myocardial infarction via histone acetylation. *Elife* 2021;**10**:e60311.
59. Miranda-Cervantes A, Fritzen AM, Raun SH, Hodek O, Møller LLV, Johann K, Deisen L, Gregorevic P, Gudiksen A, Artati A, Adamski J, Andersen NR, Sigvardsen CM, Carl CS, Voldstedlund CT, Kjøbsted R, Hauck SM, Schjerling P, Jensen TE, Cebrian-Serrano A, Jähnert M, Gottmann P, Burtscher I, Lickert H, Pilegaard H, Schürmann A, Tschöp MH, Moritz T, Müller TD, Sylow L, Kiens B, Richter EA, Kleinert M. Pantothenate kinase 4 controls skeletal muscle substrate metabolism. *Nat Commun* 2025;**16**:345.
60. Noels H, Jankowski V, Schunk SJ, Vanholder R, Kalim S, Jankowski J. Post-translational modifications in kidney diseases and associated cardiovascular risk. *Nat Rev Nephrol* 2024;**20**:495–512.
61. Liu S, Fu S, Wang G, Cao Y, Li L, Li X, Yang J, Li N, Shan Y, Cao Y, Ma Y, Dong M, Liu Q, Jiang H. Glycerol-3-phosphate biosynthesis regenerates cytosolic NAD(+) to alleviate mitochondrial disease. *Cell Metab* 2021;**33**:1974–1987.e9.
62. Tran DH, Wang ZV. Glucose metabolism in cardiac hypertrophy and heart failure. *J Am Heart Assoc* 2019;**8**:e012673.
63. Dyck JR, Cheng JF, Stanley WC, Barr R, Chandler MP, Brown S, Wallace D, Arrhenius T, Harmon C, Yang G, Nadzan AM, Lopaschuk GD. Malonyl coenzyme a decarboxylase inhibition protects the ischemic heart by inhibiting fatty acid oxidation and stimulating glucose oxidation. *Circ Res* 2004;**94**:e78–e84.
64. Bei Y, Zhu Y, Zhou J, Ai S, Yao J, Yin M, Hu M, Qi W, Spanos M, Li L, Wei M, Huang Z, Gao J, Liu C, van der Kraak PH, Li G, Lei Z, Sluijter JPG, Xiao J. Inhibition of Hmbox1 promotes cardiomyocyte survival and glucose metabolism through Gck activation in ischemia/reperfusion injury. *Circulation* 2024;**150**:848–866.
65. Steiger S, Li L, Bruchfeld A, Stevens KI, Moran SM, Floege J, Caravaca-Fontán F, Mirioglu S, Teng OYK, Frangou E, Kronbichler A; Immunonephrology Working Group (IWG) of the European Renal Association (ERA). Sex dimorphism in kidney health and disease: mechanistic insights and clinical implication. *Kidney Int* 2025;**107**:51–67.
66. Ma J, Li Y, Li P, Yang X, Zhu S, Ma K, Gao F, Gao H, Zhang H, Ma XL, Du J, Li Y. S100a8/A9 as a prognostic biomarker with causal effects for post-acute myocardial infarction heart failure. *Nat Commun* 2024;**15**:2701.
67. Forelli N, Eaton D, Patel J, Bowman CE, Kawakami R, Kuznetsov IA, Li K, Brady C, Bedi K, Yang Y, Koya K, Megill E, Kanter DS, Smith LG, Bowman GR, Snyder N, Edwards J, Margulies K, Arany Z. SGLT2 inhibitors activate pantothenate kinase in the human heart. *bioRxiv*; 2024. DOI: 10.1101/2024.07.26.605401.